論文 / 著書情報
Article / Book Information

題目(和文)	近傍銀河における星形成活動と分子ガスの関係とその環境依存性
Title(English)	Star Formation Activity and Molecular Gas across Environments in Nearby Galaxies
著者(和文)	小山舜平
Author(English)	Shuhei Koyama
出典(和文)	学位:博士(理学), 学位授与機関:東京工業大学, 報告番号:甲第10716号, 授与年月日:2018年3月26日, 学位の種別:課程博士, 審査員:松原 英雄,河合 誠之,宗宮 健太郎,堂谷 忠靖,野村 英子,小麥 真也
Citation(English)	Degree:Doctor (Science), Conferring organization: Tokyo Institute of Technology, Report number:甲第10716号, Conferred date:2018/3/26, Degree Type:Course doctor, Examiner:,,,,,
学位種別(和文)	博士論文
Type(English)	Doctoral Thesis

Star Formation Activity and Molecular Gas across Environments in Nearby Galaxies

Shuhei KOYAMA

February 2018

Abstract

Galaxies in the local universe reside in various environments such as clusters, groups or fields. It is widely recognized that galaxy properties are strongly dependent on their surrounding environment. For example, the fraction of passive early-type galaxies increases with local galaxy number density, while that of young, star-forming late-type galaxies decreases. These strong correlations between galaxy properties and environment suggest that there exist some mechanisms which accelerate galaxy growth and/or efficient quenching of star formation in high-density environments—so called "environmental effect (or environmental quenching)". However, the physical mechanisms responsible for the environmental effect are still unclear, and identifying the key mechanism(s) which drives galaxy evolution in high-density environment is one of the most important goals of the modern extra-galactic astronomy.

To reveal these mechanisms, we present the molecular gas mass fraction ($f_{\rm H_2} = M_{\rm H_2}/M_*$) and star formation efficiency ($SFE = SFR/M_{\rm H_2}$) of local galaxies at $z = 0.025 - 0.16$ on the basis of our new CO($J = 1 - 0$) observations with the Nobeyama 45m radio telescope, combined with the COLDGASS catalog, as a function of galaxy environment defined by the local number density of galaxies measured with SDSS DR7 spectroscopic data. As a result, we revealed that both $f_{\rm H_2}$ and SFE have strong positive correlations with the SFR offset from the star-forming main sequence (ΔMS),

and most importantly, we find that these correlations are universal across all environments. Further, we also confirmed that even if we took the systematics, i.e. the influence of undetected CO spectra, gas metallicity- and ΔMS-dependent $\alpha_{\rm CO}$, and adoption of another definition of environment: halo mass (M_h), into account, our findings were unchanged.

Our results demonstrate that the average $f_{\rm H_2}$ and SFE are determined by the average ΔMS of the sample, regardless their surrounding environment. Since the average ΔMS strongly depends on environment, it is not surprising to see the environmental dependence of average $f_{\rm H_2}$ and SFE if the samples are selected randomly without considering their ΔMS distribution. In other words, our results suggest that $f_{\rm H_2}$ and SFE do not depend on environment at fixed ΔMS. We therefore expect that the apparently different suggestions made by different authors in the literature regarding the environmental impacts on the molecular gas content in galaxies can be originated by their different sample selection.

Based on our observational results, we conclude that the star formation process occurring within individual galaxies is not strongly affected by their global environment, but primarily controlled by their molecular gas content. In other words, our results suggest that the role of environment is to reduce the gas reservoir in galaxies. To maintain the universal ΔMS–$f_{\rm H_2}$ and –SFE correlations, the mechanism(s) responsible for the environmental effects must reduce the molecular gas in longer time-scale than that of star formation. Following this requirement, we infer that the suppression of molecular gas supply through atomic gas stripping or strangulation would be the most plausible mechanism responsible for the environmental effects.

Contents

Chapter 1

Introduction

1.1 Galaxy Evolution

Star-forming galaxies have a tight positive correlation between stellar mass (M_*) and star formation rate (SFR), which is so called main sequence (MS Noeske et al., 2007; Daddi et al., 2007; Elbaz et al., 2007). At the same time, passive galaxies constitute another sequence far below the MS, which is so called red sequence (RS). Namely, galaxies are distributed bimodally on M_*–SFR plane (Figure 1.1). Current consensus is that galaxies start their lives in MS, and eventually evolve into RS with quenching of star formation, which time scale is relatively quickly ($\sim$ 1Gyr), because the number of galaxies located between two sequence (i.e. green-valley galaxies) are much small (Faber et al., 2007). Therefore, it is believed that there are some mechanisms inducing quenching of star formation.

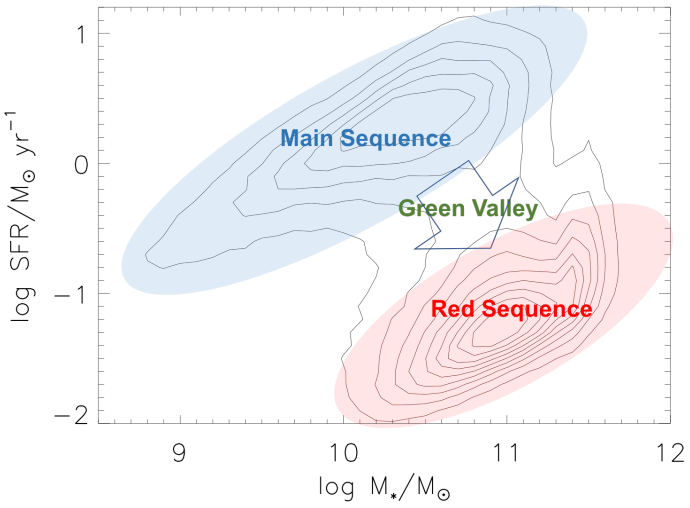

Figure 1.1: The contour shows the distribution of local galaxies in SDSS.

1.2 Environmental Effects

1.2.1 General Properties

Galaxies have nonuniform distribution in the universe. In local universe, there exist various environments such as cluster, group and field, which are characterized by local galaxy number density. For example, clusters and groups have higher local number density than fields, further intergalactic/intercluster medium (IGM) in clusters or groups also has higher density and temperature than that in fields.

Galaxy properties are known to be strongly dependent on their surrounding environment. In the local universe, the fraction of early-type galaxies increases with local galaxy density, while that of late-type galaxies decreases (e.g. Dressler, 1980; Goto et al., 2003) so called morphology–density relation (Figure 1.2). Moreover, the average star-formation rate (SFR) of galaxies also decreases with increasing local galaxy density (e.g. Lewis et al., 2002; Gómez et al., 2003). These strong correlations between galaxy properties and environment suggest that the environment plays an important role in

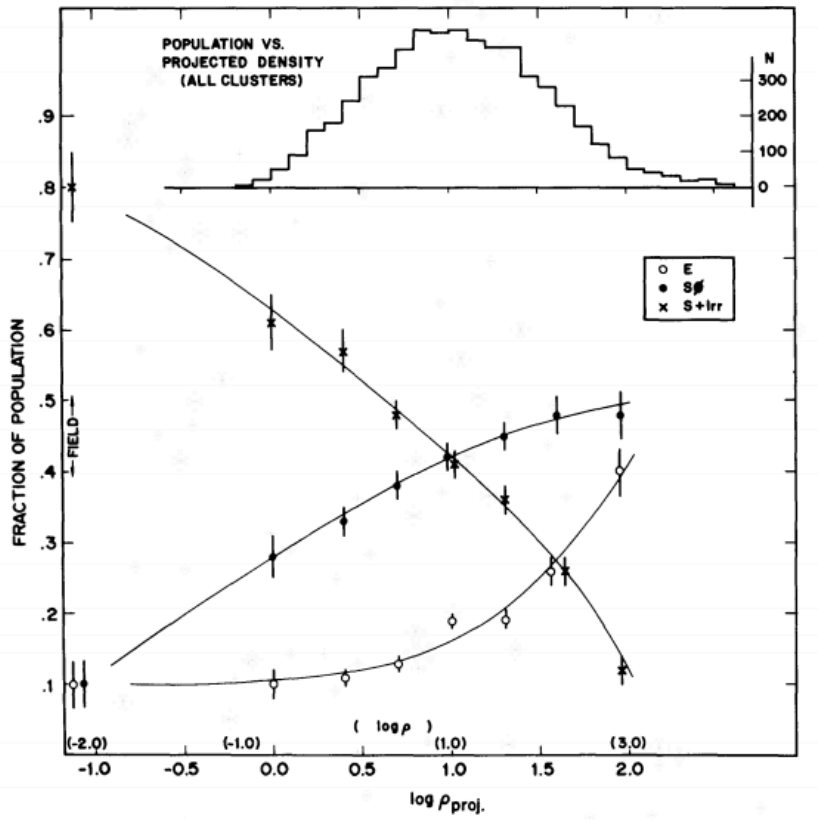

Figure 1.2: Morphology–density relation (Dressler, 1980). Horizontal axis shows the projected number density of galaxies. Vertical axis shows the fraction of each morphological types: elliptical denoted by open circle, S0 by filled circle and spiral(+ irregular) by X.

shaping the nature of individual galaxies. It is believed that there exist some mechanisms which accelerate galaxy growth and/or efficient quenching of star formation in high-density environments–so called "environmental effects (or environmental quenching)". However, the physical mechanisms responsible for the environmental effects are still unclear, and identifying the key mechanism(s) which drives galaxy evolution in high-density environment is one of the most important goals of the modern extra-galactic astronomy.

1.2.2 Proposed Mechanisms

Many physical mechanisms have been proposed to explain the environmental effects. Here, we provide the brief introductions of major proposed mechanisms for the environmental effects.

Gravitational Interaction

It was reported that tidal force among galaxies is one of the possible mechanism of environmental effects. Since its force is proportional to M/R^3, where M is the mass of neighbor galaxy and R is the separation between galaxies, it can remove gas, dust and stars from galactic halo, which is called "tidal stripping" (Spitzer & Baade, 1951). The numerical simulation by Valluri & Jog (1990) also proposed that the tidal interactions are more efficient to loose peripheral matter such as outer gas than the matters located in the inner galactic potential.

As an additional mechanism, Moore et al. (1996) proposed that high-speed galaxy-galaxy close encounters, which is called "galaxy harassment". Harassment can disturb galaxy morphology and decrease the angular momentum of their gas, which induce the infall of gas toward the galaxy center and nuclear active star formation.

Ram Pressure Stripping

Gunn & Gott (1972) proposed that if galaxies move at $\sim 1000\,\mathrm{km\,s^{-1}}$ through the hot ($\sim 10^7 - 10^8\,\mathrm{K}$) and dense ($\sim 10^3 - 10^4\,\mathrm{cm^{-3}}$) IGM, ISM can be removed from galaxies by ram pressure, which is called "ram pressure stripping". Ram pressure P is proportional to IGM density and the square of galaxy velocity relative to the IGM as follows:

$$P = \rho_{IGM} V_{gal}^2, \tag{1.1}$$

where ρ_{IGM} is the density of IGM and V_{gal} is the galaxy velocity relative to IGM. When P exceeds the gravitational pressure anchoring the gas to the disk:

$$P > 2\pi G \Sigma_{star} \Sigma_{gas}, \tag{1.2}$$

ISM is removed from galaxies, where Σ_{star} is the star surface density, and Σ_{gas} is the gas surface density. Boselli & Gavazzi (2006) proposed that for nearby three clusters (Virgo, Coma and A1376), ram pressure can effectively remove the gas from many galaxies, if they have the velocity larger than the cluster velocity dispersion.

Strangulation

Larson et al. (1980) proposed that the suppression of gas supply can shut down the star formation, which is called "strangulation". Since star-forming galaxies replenish the gas consumed by star formation from infall of an extended gas reservoir, if the gas is removed from outer galaxy halo, the star formation would exhaust the available gas, eventually quenching their star formation activity on timescales of a few Gyr.

1.2.3 Environmental Impacts on Gas in Galaxies

Because proposed mechanisms are expected to influence on gas content and/or efficiency of star formation, it is very important to investigate atomic (HI) and molecular (H_2) gas content in galaxies and their relation with star formation activity to understand the environmental effects.

For HI gas content, many studies investigated the environmental impacts on the HI gas content, showing that HI gas fraction is decreased for star-forming galaxies in cluster environment (Giovanelli & Hynes, 1985; Chung et al., 2009; Cortese et al., 2011; Serra et al., 2012) and also in group environment

(Kilborn et al., 2009; Rasmussen et al., 2012; Catinella et al., 2013; Brown et al., 2017).

These findings on the HI deficiency for star-forming galaxies in high-density environments motivate us to study the environmental impacts on their molecular gas content, which is the more direct fuel for star formation. If the molecular gas is also reduced by the environmental effects (like HI gas), then the average gas depletion time of those galaxies would become shorter, yielding more rapid consumption of molecular gas in high-density environments. In fact, there have been a number of studies investigating the environmental dependence of molecular gas content with CO observations of nearby galaxy clusters. Some pioneering work showed that cluster galaxies have amounts of molecular gas similar to those of the isolated galaxies (Kenney & Young, 1989; Casoli et al., 1991; Boselli et al., 1997; Lavezzi & Dickey, 1998). These authors claimed that the environment does not affect the molecular gas content in galaxies, because the molecular gas is more strongly bound in the central part of galaxies by the gravitational potential than HI gas. However, some recent studies reported that cluster galaxies are deficient in molecular gas content, suggesting that the molecular gas stripping takes place in cluster environment (e.g. Fumagalli & Gavazzi, 2008; Corbelli et al., 2012; Jablonka et al., 2013; Scott et al., 2013; Boselli et al., 2014). It was also reported that the cluster environment could enhance the molecular gas mass fraction (e.g. Nakanishi et al., 2006; Mok et al., 2016, 2017). For the environmental dependence of star formation efficiency, Mok et al. (2016, 2017) proposed that the cluster environment could decrease the efficiency of star formation through molecular gas heating or turbulence at the same time, while some other studies suggest an *increased* star formation efficiency due to the gas compression in cluster galaxies (e.g. Ebeling et al., 2014; Lee et al., 2017).

1.3 Research Strategy

1.3.1 Problems of Previous Studies

Our understanding of the environmental impacts on the molecular gas content and star formation efficiency in galaxies is still highly uncertain. The different results (or discrepancy) between different studies probably originate in the different sample selection, different environmental coverage, or insufficient sample size. In particular, most of the previous studies mentioned above attempted to compare the results on cluster galaxies and field galaxies. However, the average star-formation rates are known to change monotonically with environment. A more systematic study covering a wide environmental range from low- to high-density environment is needed.

It is also important to carefully select the targets for molecular gas (CO) observations. It has been shown that both molecular gas mass fraction ($f_{\rm H_2} = M_{\rm H_2}/M_*$) and star-formation efficiency ($SFE = SFR/M_{\rm H_2}$) are strongly dependent on their location in the SFR–M_* diagram (Saintonge et al., 2012; Genzel et al., 2015; Saintonge et al., 2016). Based on the extensive CO galaxy observations of nearby galaxies (COLDGASS survey), Saintonge et al. (2012) demonstrated that both $f_{\rm H_2}$ and SFE significantly increase with the SFR "offset" values from the star-forming main sequence (ΔMS), implying that star-formation activity is controlled by the molecular gas content in galaxies (Figure 1.3). It is therefore very important to pay extra attention to the ΔMS range of the sample; otherwise the results can easily be biased due to the different ΔMS range between different samples.

1.3.2 Aim of This Thesis

In this thesis, we aim to reveal the environmental effects on molecular gas content and star formation efficiency by investigating the environmental de-

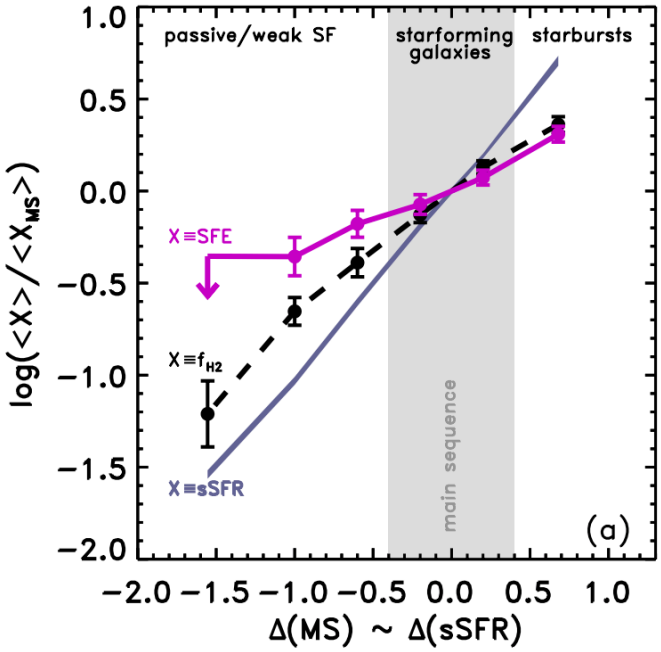

Figure 1.3: Molecular gas mass fraction ($f_{\rm H_2}$) and star formation efficiency (SFE) as a function of SFR offset from the MS (ΔMS) from the COLDGASS sample (Saintonge et al., 2012).

pendence of ΔMS–$f_{\rm H_2}$ (and –SFE) correlations, which can overcome the biases given above. In Figure 1.4, we show the schematic view of ΔMS–$f_{\rm H_2}$ correlation to explain the working hypothesis. If star formation efficiency is decreased by heating or turbulence, galaxies in high-density environment should be distributed on red region in Figure 1.4. If it is increased by molecular gas compression, or molecular gas content is rapidly reduced by stripping, they should be distributed on blue region. To investigate these correlations and verify these working hypotheses, we need the galaxy sample covering wide range of density environment and Δ MS. To achieve this, we have performed new CO observations of nearby star-forming galaxies with the Nobeyama 45m radio telescope (NRO 45m) cover wide range in ΔMS and environment. By combining our NRO 45m data with the literature data, this work provides the first systematic study on the environmental impacts on the molecular gas

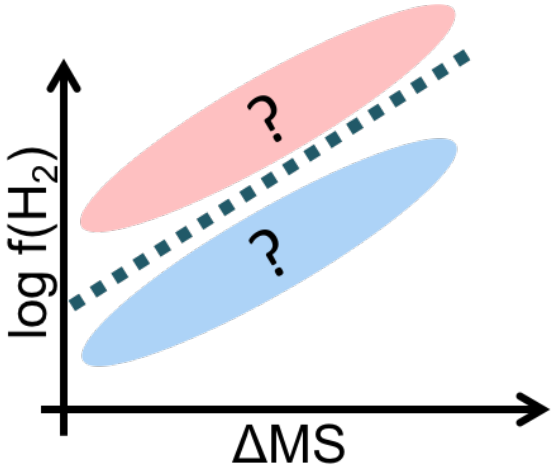

Figure 1.4: Schematic view of the correlation between ΔMS and $f_{\rm H_2}$. Dotted line indicates the correlation in general (field) environment.

content in galaxies across a wide environmental range.

This thesis is organized as follows. In Chapter 2, we describe our sample selection and our new CO observations with NRO 45m telescope, as well as our supplementary data from the COLDGASS survey. In Chapter 3, we present our main results on the environmental independence of the relation between star formation activity and molecular gas. In Chapter 4, we provide the implications for the environmental effects through comparing our results with previous studies. Finally, our conclusions are presented in Chapter 5. Throughout this thesis, we assume the ΛCDM universe with $H_0 = 70$ km s^{-1} Mpc^{-1}, $\Omega_m = 0.3$ and $\Omega_\Lambda = 0.7$, and Kroupa (2001) initial mass function (IMF).

Chapter 2

Data

Here, we describe the sample construction for the study of environmental impacts on molecular gas. First, we introduce the SDSS catalog, which is the parent population for this thesis (Section 2.1) and the definition of environment (Section 2.2). Then, we introduce the CO(1–0) sample, which includes the data we observed at NRO 45m telescope (Section 2.3) and the archive data (Section 2.4). Finally, we summarize the final sample in Section 2.5.

2.1 Sloan Digital Sky Survey

The Sloan Digital Sky Survey (York et al., 2000, SDSS) is the most large-scale optical imaging and spectroscopic survey by the 2.5 m ground telescope in the history of astronomy. The imaging survey covers one-quarter of the sky in five broad bands (u, g, r, i and z) with 95% completeness limits of 22.0, 22.2, 22.2, 21.3 and 20.5 mag, respectively. The spectroscopic survey covers the wavelength rage of $3800-9200$ Å at $R \sim 1800$ and provides us spectra for $\sim 10^6$ galaxies, 100,000 quasars, 30,000 stars, and 30,000 serendipity targets. In this thesis, we utilize the SDSS Data Release 7 (Abazajian et al., 2009, DR7) for the parent population.

2.1.1 Star Formation Rate

SFRs for the SDSS galaxies were computed by Max Plank Institute for Astrophysics–John Hopkins University (MPA–JHU) group and published in the SDSS value-added catalog[1]. The SFRs were derived from the SDSS spectra, mainly Hα emission line luminosity for star-forming galaxies (see Brinchmann et al. (2004) for details). For the galaxies with weak Hα emission, they estimated the SFRs from 4000 Å break (D4000), which is defined as the ratio between the average flux density at λ=4050–4250 Å and λ=3750–3950 Å. They constructed the correlation between D4000 and specific SFR ($sSFR = SFR/M_*$) using the star-forming galaxies, and estimated the SFRs by applying this correlation to Hα-weak galaxies.

Since SDSS spectroscopic observations were performed by the 3 arcsec diameter fiber, these spectra cannot cover the whole region of galaxies at low-redshift ($z \lesssim 0.5$). Thus, the SFRs derived from SDSS spectra needed to be corrected for aperture effects. This aperture corrections were performed by constructing the distribution of sSFR at a given (g-r, r-i) inside the fiber, and then applying to the photometry outside the fiber for each galaxy.

2.1.2 Stellar Mass

We also use M_* of galaxies published in the MPA–JHU catalog. This M_* were obtained from the SED model fitting to the SDSS photometries (Kauffmann et al., 2003; Gallazzi et al., 2005). SED models were made from single stellar population (SSP) synthesis described in Bruzual & Charlot (2003), which constructs stellar SEDs by assuming star formation history, initial mass function and metallicity. For each model, a likelihood was calculated from χ^2, and then plausible M_* was determined from the likelihood distribution.

[1] `http://wwwmpa.mpa-garching.mpg.de/SDSS/DR7/`

2.2 Definitions of Environment

We defined the galaxy environment based on the local number density of galaxies calculated by Matsuki et al. (2017), who computed the local density of 738,143 galaxies selected from SDSS DR7 spectroscopic data within the area of $105° < R.A. < 270°$ and $-5 < DEC. < 75°$. The local number density of each galaxy (Σ_5) was calculated using the projected distance to the fifth-nearest neighbor galaxy within a velocity window of ± 1000 km s^{-1}, which corresponds to a redshift slice of $\Delta z = \pm 0.003$, and is expressed as:

$$\Sigma_5 = \frac{5}{\pi D_{p,5}^2} \, [\mathrm{Mpc}^{-2}], \tag{2.1}$$

where $D_{p,5}$ is the projected comoving distance to the fifth-nearest neighbor galaxy. To take into account the redshift dependence on the completeness limit of SDSS spectroscopic survey, Σ_5 was normalized by the median density measured within the same velocity window:

$$\rho_5 = \frac{\Sigma_5}{\langle \Sigma_5 \rangle}. \tag{2.2}$$

Figure 2.1 shows the density distribution for all the SDSS sample in the above R.A./Dec. range. Our sample covers roughly two orders of magnitude in terms of the local galaxy density. As shown in Figure 2.1, we divide the sample into five environmental bins (D1–D5) based on the following criteria: $\log \rho_5 \leq -0.6$ for D1, $-0.6 < \log \rho_5 \leq -0.2$ for D2, $-0.2 < \log \rho_5 \leq 0.2$ for D3, $0.2 < \log \rho_5 \leq 0.6$ for D4, $0.6 < \log \rho_5$ for D5. The majority of galaxies are located in D3 bin, while the galaxies in D1 and D5 bins are rare. Figure 2.2 shows the distribution of ΔMS of galaxies for each environmental bin. This plot demonstrates that our definition of environment works reasonably well, and the relative fraction of passive and star-forming galaxies clearly changes with environment. Figure 2.3 shows the spatial distribution of galaxies at $z = 0.06 - 0.07$ on the sky, to visually demonstrate that our

local density measurement can robustly trace from rich clusters as well as the filamentary large-scale structures to low-density fields.

2.3 Molecular Gas Mass Estimate

2.3.1 CO Molecule

Since molecular gas is a direct fuel for star formation, its properties are important information for galaxy evolution. To calculate the $f_{\mathrm{H_2}}$ and SFE, we have to estimate molecular gas mass. However, hydrogen molecule $\mathrm{H_2}$, which is the primary molecular gas constituent, does not have permanent electric dipole moment because it is homonuclear molecule. Therefore, dipolar rotational transitions are forbidden. It is also difficult to observe rotational quadrupole transition in mid-IR ($\sim 150 - 250\,\mathrm{K}$), because typical temperature of the molecular gas is too cold ($T \sim 10\,\mathrm{K}$) to excite these transition.

For these reasons, molecular gas mass of galaxies are generally estimated by observing rotational transitions of carbon monoxide (CO), which is the second abundant molecule. The CO rotational transition $J = 0 \rightarrow 1$ is easily excited in cold molecular gas, because this transition can be excited above $h\nu/k = 5.5\,\mathrm{K}$ and critical density is $1.1 \times 10^3\,\mathrm{cm^{-3}}$. Therefore, it is believed that CO(1–0) emission line is the good tracer for molecular gas mass. In fact, molecular gas mass $\mathrm{M_{H_2}}$ is estimated by multiplying CO luminosity L'_{CO} and CO-to-$\mathrm{H_2}$ conversion factor α_{CO} as follows:

$$M_{\mathrm{H_2}}\,[\mathrm{M_\odot}] = \alpha_{\mathrm{CO}}[\mathrm{M_\odot}(\mathrm{K\,km\,s^{-1}\,pc^2})^{-1}]L'_{\mathrm{CO}}[\mathrm{K\,km\,s^{-1}, pc^2}]. \tag{2.3}$$

In this thesis, we adopt a constant value of $\alpha_{\mathrm{CO}} = 4.3$, which is commonly used in studies of star-forming galaxies in the local universe (Bolatto et al., 2013). Although some recent studies suggested that α_{CO} could be dependent on the strength of UV radiation field, metallicity, and gas density, we will

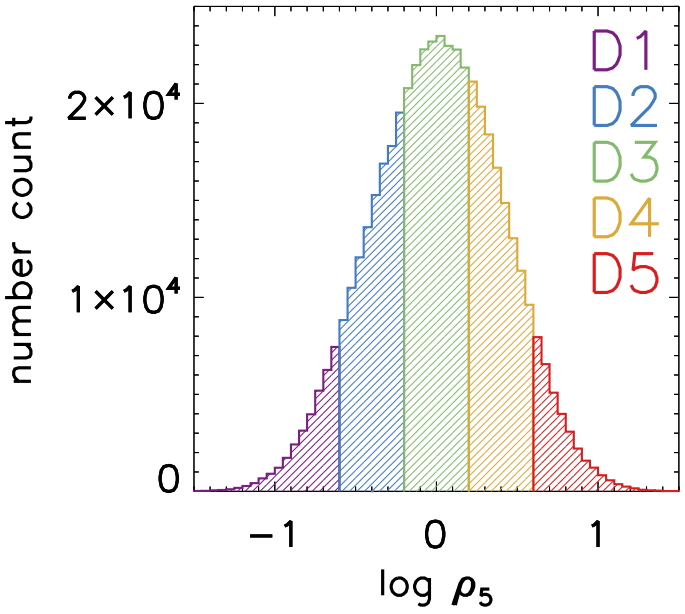

Figure 2.1: The distribution of ρ_5 for all the SDSS DR7 sample within $105° < R.A. < 270°$ and $-5 < DEC. < 75°$ computed by Matsuki et al. (2017). In this thesis, we define the environment based on ρ_5, and our definition of D1–D5 environment bins are shown with different color shades in this diagram.

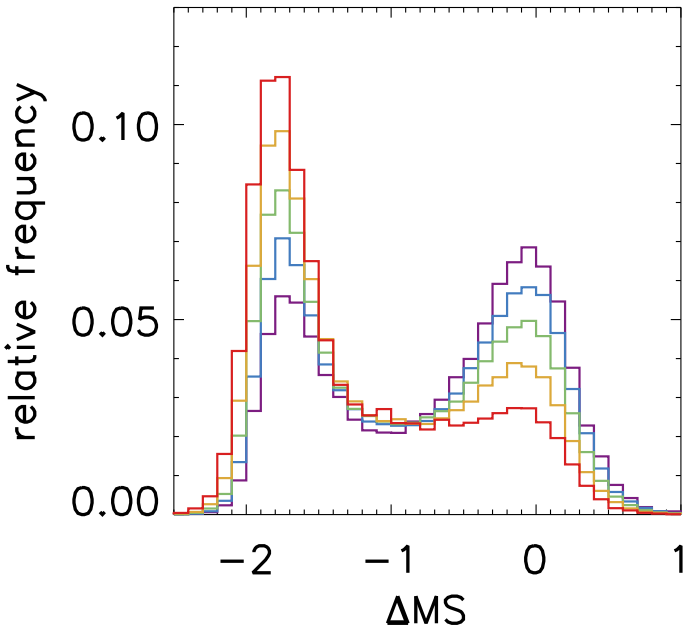

Figure 2.2: The relative frequency of ΔMS for each environmental bin.

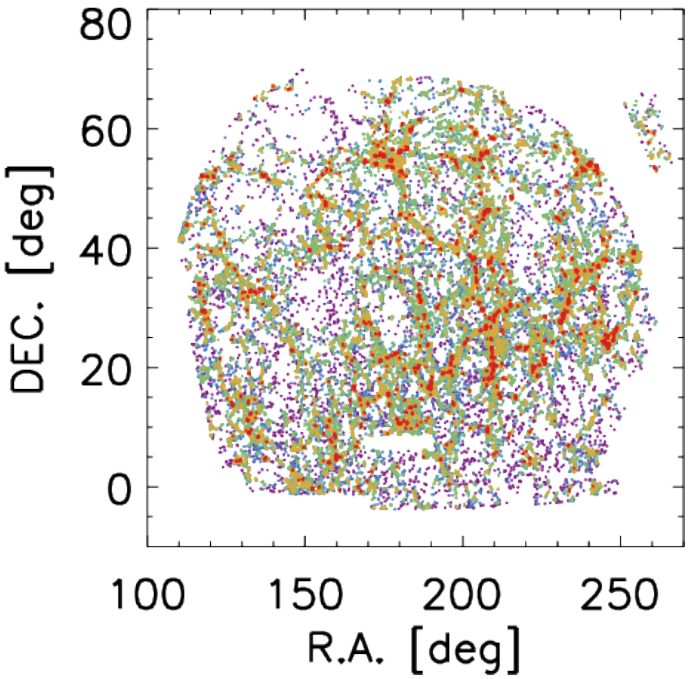

Figure 2.3: The spatial distribution of the sample galaxies at $z = 0.06 - 0.07$ on the sky. The color coding indicates different environmental bin (redder colors indicate higher-density environment).

verified that our results are unchanged even if we apply such non-constant $\alpha_{\rm CO}$ (see more details in Section 3.4).

2.3.2 Sample Selection

The goal of this thesis is to understand the environmental impact on molecular gas within galaxies across a wide environmental range. Ideally, the sample should be selected uniformly from D1–D5. Here, we explain the sample selection for CO observations at the NRO 45m telescope. We note that we have performed observations over two semesters (2015 and 2016 semester), based on different sample selection criteria so that we can obtain CO spectra for galaxies covering a wide environmental range as well as a wide ΔMS range.

2015 semester

Using the SDSS galaxies for which the local density measurements are available, we selected the target galaxies for the CO observation with NRO 45m telescope based on the following criteria:

1) To select SF galaxies, we restricted the sample to those satisfying $EW_{\rm H\alpha} > 4$Å, and adopted the SF galaxy criteria defied by Kewley et al. (2001) on the BPT diagram (Baldwin et al., 1981).

2) We selected galaxies with $z \geq 0.03$ so that the major part of galaxies are covered with a single beam size of NRO 45m telescope. The beam size of NRO 45m at 110 GHz is 15 arcsec, which corresponds to 10 kpc at $z = 0.03$.

3) We selected galaxies with $L_{IR} \geq 10^{11}$ L$_\odot$ (i.e. with Luminous Infrared Galaxies (LIRGs) class luminosity), in order to complement the COLDGASS sample which mostly covers the galaxies on and below the SF main sequence

(see Section 2.4 for details). The L_{IR}s were computed by Koyama et al. (2015) following Takeuchi et al. (2010) using *AKARI* far-IR photometric bands (Kawada et al., 2007); WIDE-S (90 μm) and WIDE-L (140 μm).

We found 1,568 galaxies satisfying the above criteria, from which we finally selected 32 targets (6–7 galaxies for each D1–D5 bin) considering the visibility from the NRO 45m telescope. The properties of our NRO 45m target galaxies are summarized in Table 2.1. We note that our sample does not necessarily cover very rich cluster environments, but we stress again that our main aim here is to "bridge" previous studies focusing on cluster and field environments, by applying a continuous environmental coverage from low- to high-density environments quantified with the local galaxy density.

2016 semester

In the 2015 semester, we focused on actively star forming galaxies in order to complement the COLDGASS sample. We also recognized that there were a lack of galaxies at low ΔMS regime in the D1 environment, and we took additional CO data in the 2016 semester. We selected 11 target galaxies in the D1 environment with the same criteria as for the 2015 semester, but here we applyied $-2 < \Delta\mathrm{MS} < -1$ instead of (3) for the 2015 semester. The properties of our target galaxies are summarized in Table 2.2.

2.3.3 CO observations

We performed CO(1–0) observations of 32 and 11 galaxies in the 2015 and 2016 semester using the NRO 45m telescope (CG151005: Y. Koyama et al., CG161017: S, Koyama et al.), respectively. The CO emission line of the rest-frame 115.271 GHz is shifted to 99.372 – 111.914 GHz according to the redshifts of our sample. We used a two-beam, two-polarization, sideband-separating SIS receiver, TZ (Nakajima et al., 2013), and a copy of a part of

Table 2.1: Summary of physical quantities of our NRO 45m sample for 2015 semester. The asterisks in the SFR column denote the galaxies for which we replaced their SFRs with the SFRs derived from L_{IR} we computed from AKARI FIR photometry (see text). We assign 0.3-dex uncertainties for these two sources, which corresponds to the typical error of the *AKARI* WIDE-L band photometry.

SDSS ID	Env.	$\log \rho_5$	z	$\log SFR\,[\mathrm{M_\odot\ yr^{-1}}]$	$\log M_*\,[\mathrm{M_\odot}]$	$\log L_{IR}\,[\mathrm{L_\odot}]$
J082656.14+040503.5	D1-1	-1.14	0.056	$0.75^{+0.24}_{-0.19}$	$10.77^{+0.10}_{-0.08}$	11.23
J133223.99+110620.4	D1-2	-1.13	0.031	$0.67^{+0.18}_{-0.09}$	$10.03^{+0.15}_{-0.10}$	11.19
J103009.77+093505.8	D1-3	-0.99	0.084	$1.30^{+0.10}_{-0.09}$	$10.89^{+0.09}_{-0.09}$	11.50
J082919.82+061744.8	D1-4	-0.96	0.048	$1.27^{+0.04}_{-0.05}$	$10.68^{+0.10}_{-0.10}$	11.06
J083948.87+263402.7	D1-5	-0.84	0.069	$0.88^{+0.14}_{-0.14}$	$10.50^{+0.08}_{-0.13}$	11.20
J140757.00+321249.2	D1-6	-0.83	0.087	$0.94^{+0.17}_{-0.14}$	$10.61^{+0.09}_{-0.09}$	11.62
J153907.86+140123.0	D2-1	-0.57	0.038	$0.89^{+0.13}_{-0.10}$	$10.40^{+0.11}_{-0.09}$	11.02
J102449.68+053327.1	D2-2	-0.46	0.067	$0.77^{+0.39}_{-0.19}$	$10.68^{+0.13}_{-0.09}$	11.30
J140132.89+305242.3	D2-3	-0.43	0.072	$1.07^{+0.11}_{-0.13}$	$10.69^{+0.10}_{-0.09}$	11.44
J122104.98+113752.3	D2-4	-0.40	0.068	$1.44^{+0.21}_{-0.14}$	$10.87^{+0.16}_{-0.10}$	11.81
J095804.35+124414.3	D2-5	-0.27	0.062	$1.10^{+0.04}_{-0.11}$	$10.07^{+0.11}_{-0.10}$	11.26
J095545.86+314840.1	D2-6	-0.21	0.084	$1.34^{+0.09}_{-0.10}$	$11.03^{+0.11}_{-0.10}$	11.49
J091528.96+202754.5	D3-1	-0.18	0.068	$1.02^{+0.19}_{-0.16}$	$10.72^{+0.10}_{-0.08}$	11.22
J155725.27+244332.1	D3-2	-0.08	0.041	$0.79^{+0.18}_{-0.12}$	$10.57^{+0.09}_{-0.08}$	11.05
J102420.51+035911.9	D3-3	-0.02	0.099	$1.30^{+0.22}_{-0.13}$	$11.00^{+0.13}_{-0.11}$	11.61
J101410.56+342034.7	D3-4	0.02	0.038	$1.00^{+0.39}_{-0.12}$	$10.34^{+0.14}_{-0.12}$	11.20
J115801.99+103136.2	D3-5	0.09	0.065	$1.15^{+0.12}_{-0.13}$	$10.61^{+0.10}_{-0.09}$	11.56
J095835.38+004434.0	D3-6	0.12	0.065	$1.35^{+0.14}_{-0.12}$	$10.80^{+0.09}_{-0.09}$	11.34
J110319.65+151202.4	D4-1	0.23	0.136	$1.56^{+0.30}_{-0.30}$*	$11.04^{+0.10}_{-0.10}$	11.32
J110326.80+161820.8	D4-2	0.36	0.068	$1.11^{+0.12}_{-0.09}$	$11.04^{+0.13}_{-0.09}$	11.20
J123932.01+272950.4	D4-3	0.37	0.057	$1.22^{+0.12}_{-0.10}$	$10.86^{+0.09}_{-0.09}$	11.21
J103422.30+442349.2	D4-4	0.37	0.052	$0.83^{+0.09}_{-0.10}$	$10.43^{+0.09}_{-0.10}$	11.31
J101632.22+085842.9	D4-5	0.40	0.103	$1.10^{+0.13}_{-0.10}$	$10.61^{+0.09}_{-0.08}$	11.70
J103014.76+110415.8	D4-6	0.41	0.065	$1.08^{+0.14}_{-0.10}$	$10.81^{+0.10}_{-0.09}$	11.32
J142343.69+064441.3	D4-7	0.59	0.157	$1.30^{+0.17}_{-0.16}$	$10.89^{+0.10}_{-0.10}$	11.05
J090105.72+343526.2	D5-1	0.61	0.065	$2.08^{+0.30}_{-0.30}$*	$10.21^{+0.09}_{-0.11}$	11.84
J102601.79+213537.6	D5-2	0.64	0.042	$0.66^{+0.12}_{-0.10}$	$10.41^{+0.09}_{-0.08}$	11.01
J095725.12+004351.3	D5-3	0.67	0.087	$1.48^{+0.13}_{-0.12}$	$11.02^{+0.10}_{-0.08}$	11.46
J144352.34+162827.2	D5-4	0.67	0.054	$1.04^{+0.16}_{-0.11}$	$10.61^{+0.11}_{-0.08}$	11.25
J090509.86+172557.9	D5-5	0.76	0.067	$1.11^{+0.11}_{-0.10}$	$10.68^{+0.09}_{-0.09}$	11.32
J151604.07+195134.5	D5-6	0.83	0.049	$1.34^{+0.17}_{-0.09}$	$10.74^{+0.11}_{-0.09}$	11.21
J142306.89+204324.0	D5-7	1.14	0.049	$0.83^{+0.19}_{-0.17}$	$10.91^{+0.09}_{-0.09}$	11.22

Table 2.2: Summary of physical quantities of our NRO 45m sample in 2016 semester.

SDSS ID	Env.	$\log \rho_5$	z	$\log SFR\,[\mathrm{M_\odot\,yr^{-1}}]$	$\log M_*\,[\mathrm{M_\odot}]$
J104025.88+112937.1	D1p-1	-0.60	0.040	$-0.60^{+0.47}_{-0.65}$	$10.43^{+0.09}_{-0.10}$
J110230.07+184706.5	D1p-2	-0.88	0.034	$-0.70^{+0.44}_{-0.58}$	$10.32^{+0.09}_{-0.09}$
J110809.35+130237.6	D1p-3	-0.67	0.037	$-0.42^{+0.52}_{-0.84}$	$10.94^{+0.09}_{-0.09}$
J141044.28+185737.9	D1p-4	-0.60	0.038	$-0.87^{+0.45}_{-0.31}$	$10.01^{+0.11}_{-0.10}$
J105729.75+190305.4	D1p-5	-0.80	0.045	$-0.95^{+0.56}_{-0.78}$	$10.76^{+0.09}_{-0.09}$
J113105.76+223110.9	D1p-6	-0.62	0.047	$-1.19^{+0.66}_{-0.84}$	$10.82^{+0.09}_{-0.09}$
J114434.32+230551.7	D1p-7	-0.63	0.047	$-0.35^{+0.54}_{-0.84}$	$10.84^{+0.10}_{-0.10}$
J133808.64+192054.9	D1p-8	-0.99	0.036	$-1.12^{+0.61}_{-0.79}$	$10.81^{+0.09}_{-0.09}$
J133345.35+235137.4	D1p-9	-0.72	0.037	$-1.25^{+0.60}_{-0.80}$	$10.57^{+0.09}_{-0.09}$
J140323.04+175849.7	D1p-10	-0.75	0.038	$-1.10^{+0.58}_{-0.80}$	$10.71^{+0.09}_{-0.09}$
J142607.68+192300.2	D1p-11	-0.70	0.044	$-0.77^{+0.75}_{-0.92}$	$10.84^{+0.12}_{-0.11}$

the FX-type correlator for the Atacama Compact Array, SAM45 (Kamazaki et al., 2012). Typical on-source integration time was 1.5 (3) hours for each galaxy in 2015 (2016), respectively. During the observation, the pointing accuracy was checked every hour by observing SiO maser sources at 43 GHz. The image rejection ratio (IRR) was measured for each target and for each observing date, and the IRR values were 5 – 30 dB at the center of the intermediate frequency. The system noise temperature ($T_{\rm sys}$) of our observation ranges between 100 – 540 K with the median $T_{\rm sys}$ value of 150 K.

2.3.4 Data Reduction

The flux calibration was performed by the chopper wheel method and the measured IRR scaling factor (f):

$$f = 1 + \frac{1}{10^{IRR/10}}. \tag{2.4}$$

The main beam temperature ($T_{\rm mb}$) was calculated by $T_{\rm mb} = T_a^*/\eta_{\rm mb}$, where T_a^* is the antenna temperature. The main beam efficiency ($\eta_{\rm mb}$) during the semester was 0.44 according to the NRO website[2].

[2] http://www.nro.nao.ac.jp/~nro45mrt/html/prop/eff/eff_latest.html

Data reduction was performed by using the NEWSTAR software, which was developed by NRO based on the Astronomical Image Processing System (AIPS) package. We used the observed data with wind velocities of $< 5\,\mathrm{m\,s^{-1}}$, pointing accuracy better than $5''$, $T_{\rm sys}$ better than 300 K, and IRR values larger than 7 dB. We also extracted the data with the rms noise temperature levels of $(T_{\rm rms}) > 0.045\,\mathrm{K}$ in the $T_{\rm mb}$ scale at a velocity resolution of $200\,\mathrm{km\,s^{-1}}$ to exclude bad baseline spectra. Then, we subtracted baselines by linear fitting and sum up for both polarizations. After binning up to $40\,\mathrm{km\,s^{-1}}$ resolution, we calculated the integrated intensity $I_{\rm CO}$ according to $I_{\rm CO} = \int T_{\rm mb}\,dv$. The error in $I_{\rm CO}$ was calculated according to $T_{\rm rms}\sqrt{\Delta V_{\rm e}\Delta v}$, where $\Delta V_{\rm e}$ is the full line width of CO spectra. The $T_{\rm rms}$ at the velocity resolution of $\Delta v = 40\,\mathrm{km\,s^{-1}}$ is 2.1–8.5 and 1.8–4.5 mK ($T_{\rm mb}$) in 2015 and 2016 semester, respectively. We detected CO emission line from 40 target galaxies with the signal (peak temperature) -to-noise (rms) ratio (S/N) of 3 – 17, however there are three undetected sources ($S/N < 3$) in 2016 semester. Finally, we calculate the CO luminosity ($L'_{\rm CO}$) based on the following equation:

$$L'_{\rm CO} = \frac{\Omega_b I_{\rm CO} D_L^2}{(1+z)^3}\ [\mathrm{K\ km\ s^{-1}\ pc^2}], \tag{2.5}$$

where $\Omega_{\rm b}$ is the beam solid angle of $\theta_{\rm mb}$, and D_L is the luminosity distance. For undetected sources, we estimated the 3σ upper limits assuming $400\,\mathrm{km\,s^{-1}}$ velocity width. The observational results are summarized in Table 2.3 and 2.4, and the observed CO spectra are shown in Figure 2.4–2.10.

2.4 CO Archive Data

In this study, we also use the CO data of nearby galaxies publicly available from the COLDGASS survey (Saintonge et al., 2011, 2012). The COLDGASS is one of the most extensive extragalactic CO surveys performed with the

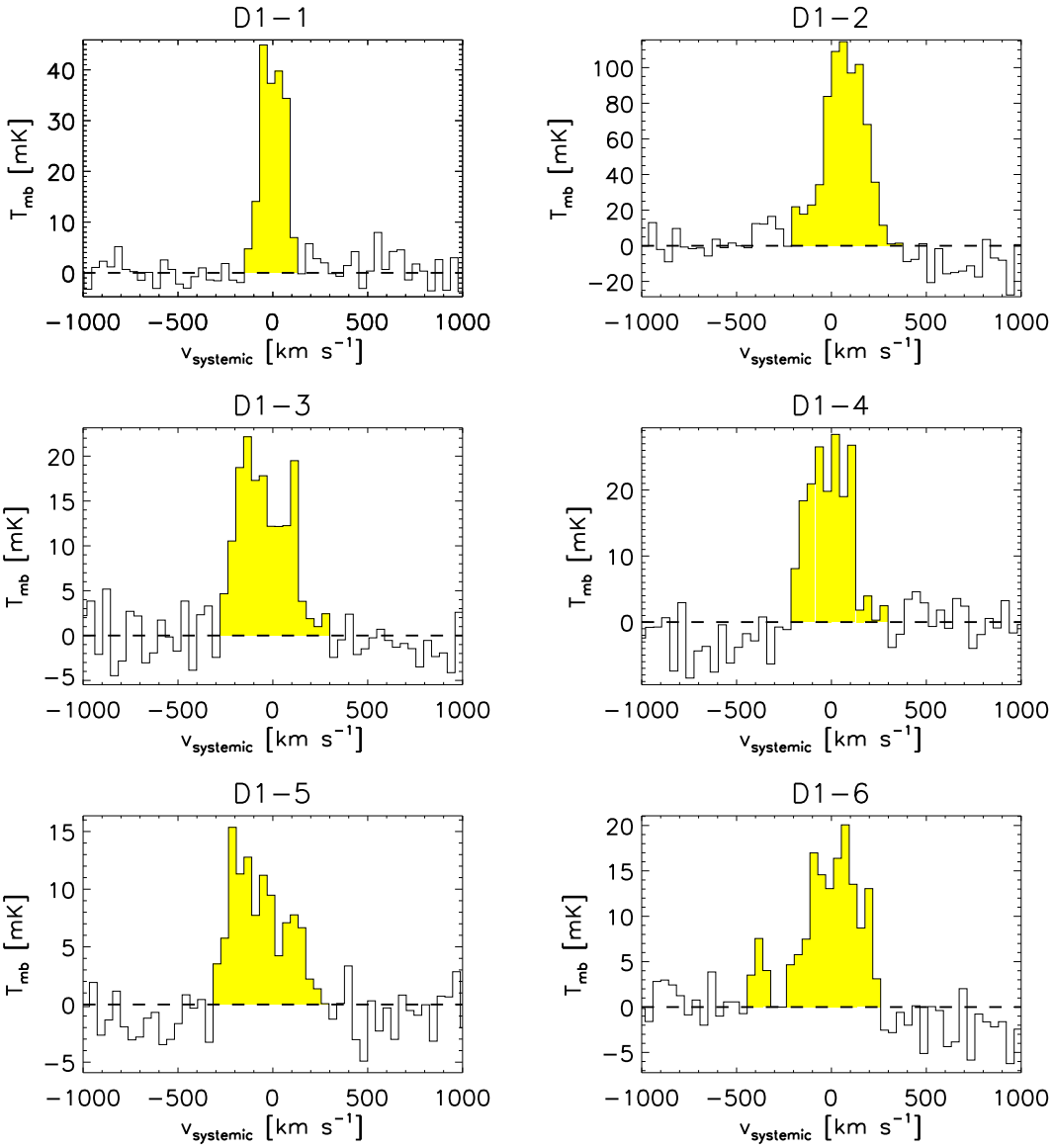

Figure 2.4: The CO spectra of D1 galaxies derived with our NRO 45m observations in 2015 semester. The CO flux of each galaxy is calculated by summing the intensity within the velocity range colored in yellow. Their physical properties are summarized in Table 2.3.

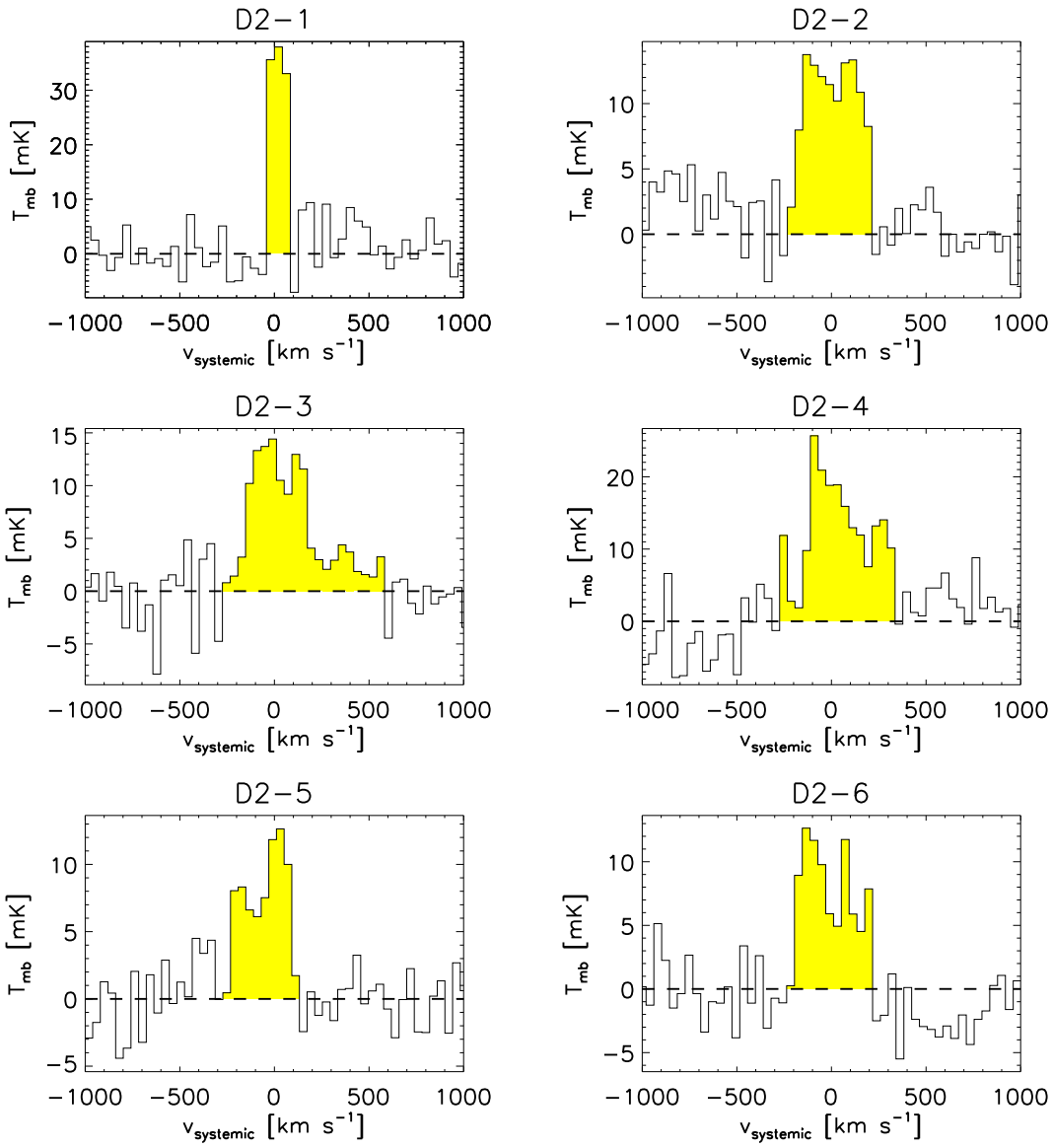

Figure 2.5: The CO spectra of D2 galaxies.

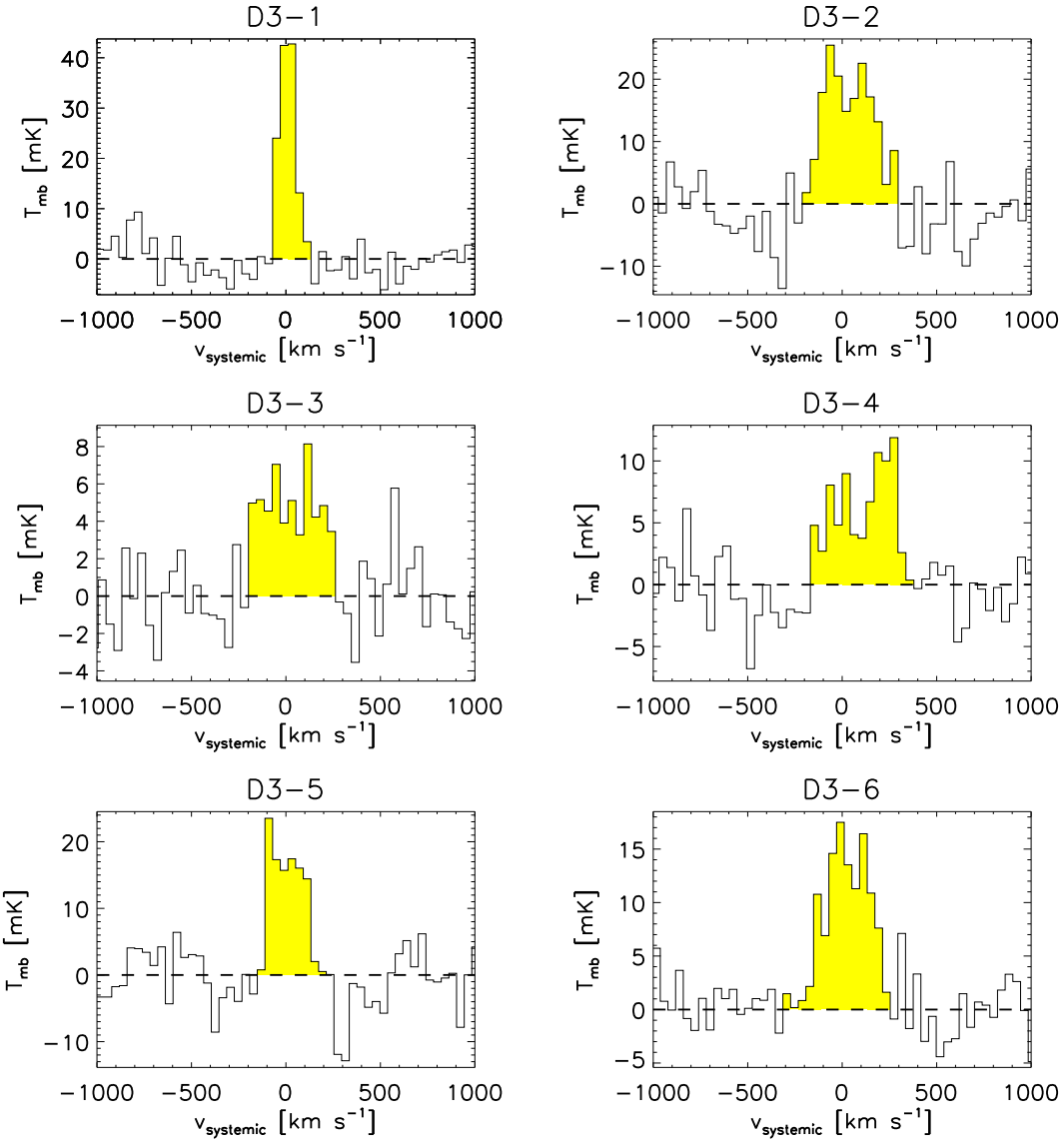

Figure 2.6: The CO spectra of D3 galaxies.

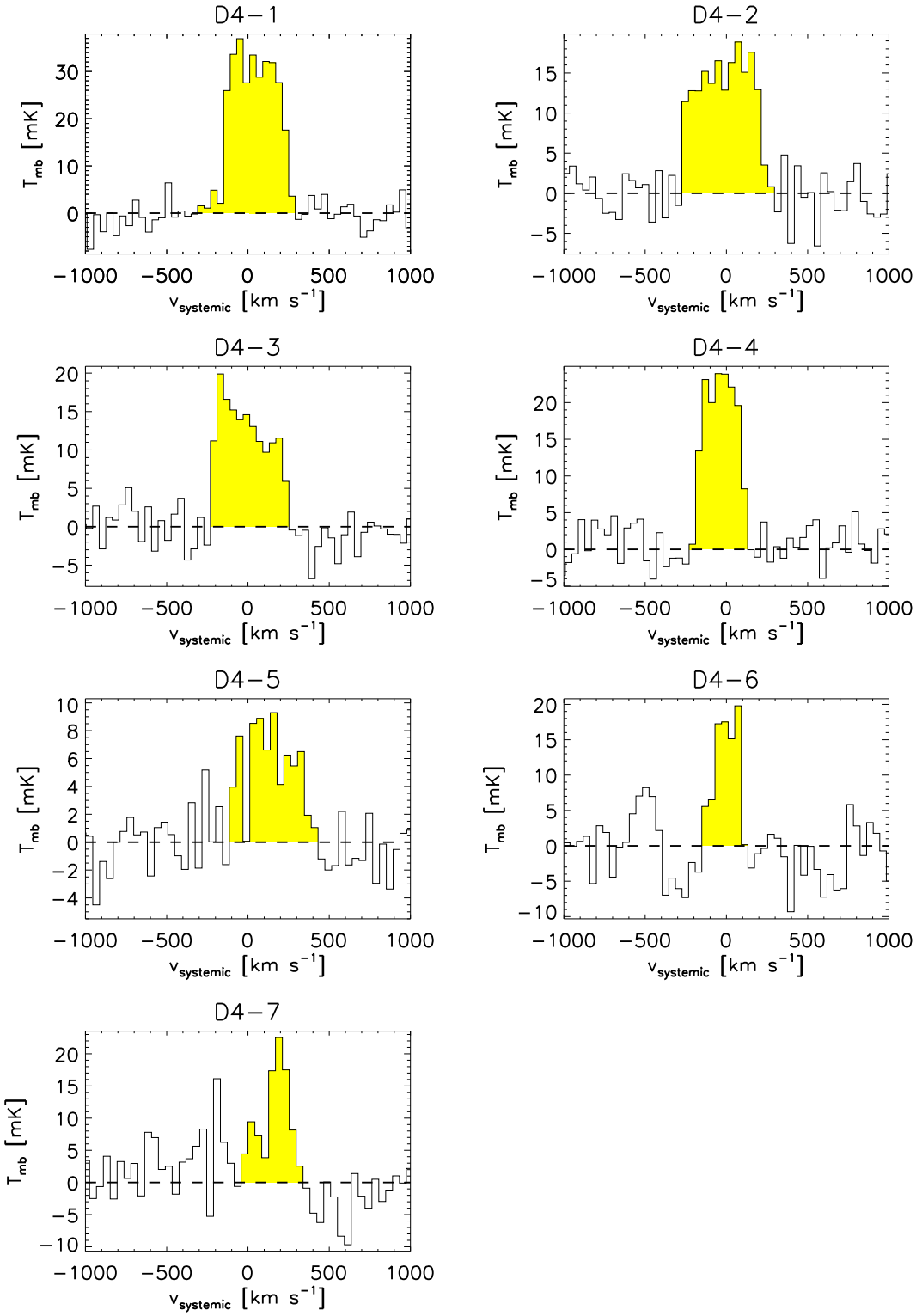

Figure 2.7: The CO spectra of D4 galaxies.

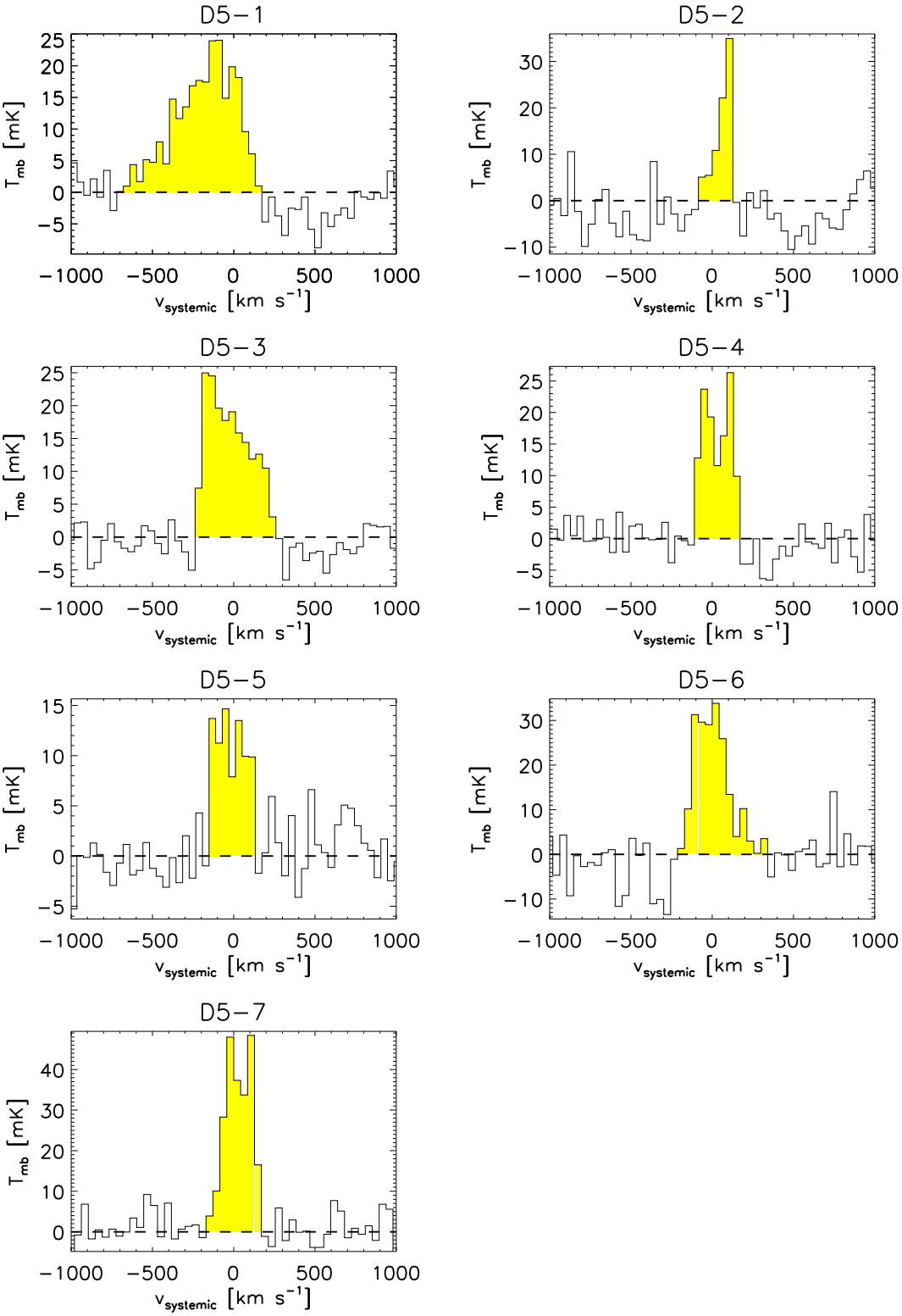

Figure 2.8: The CO spectra of D5 galaxies.

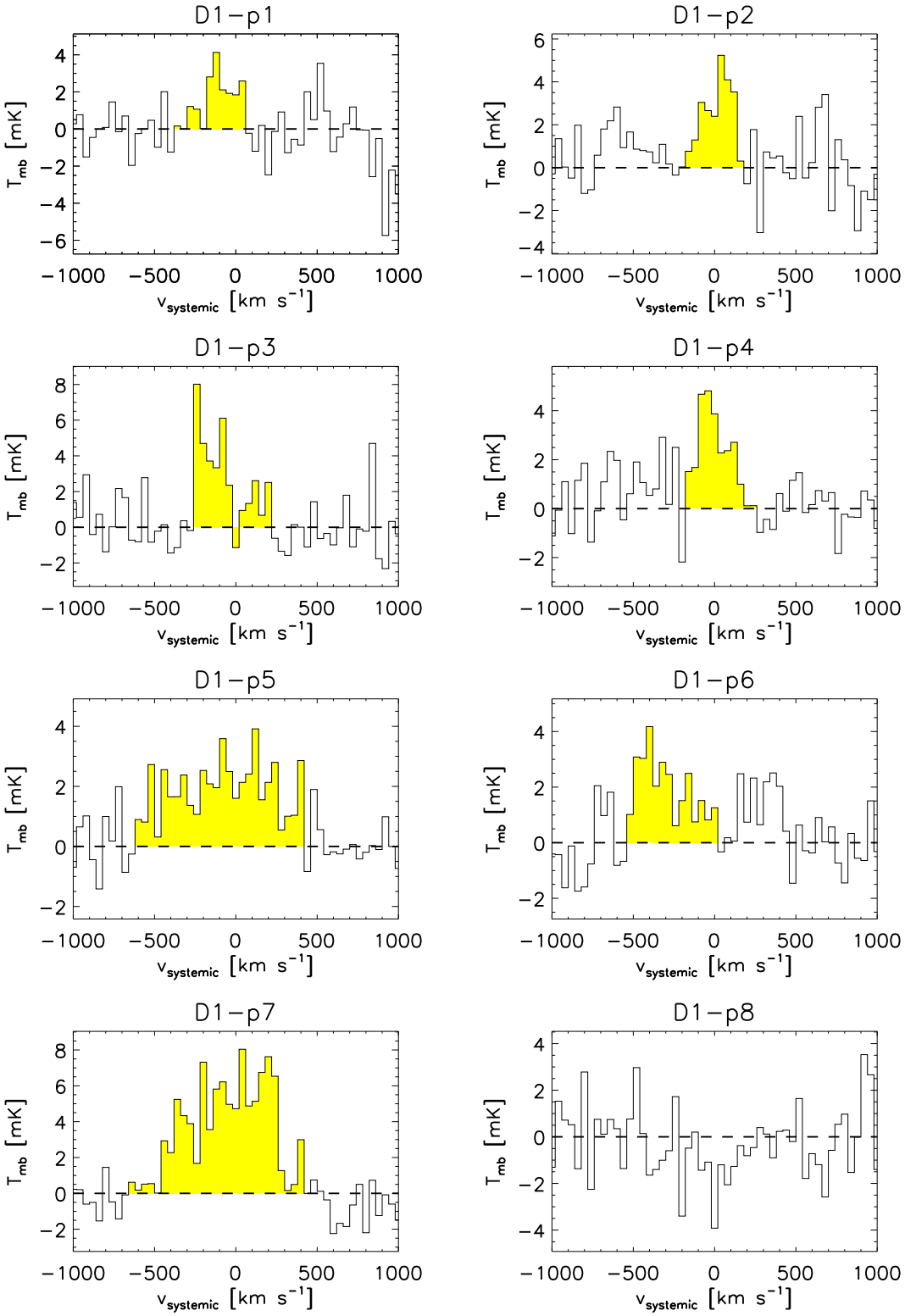

Figure 2.9: The CO spectra of D1 passive galaxies taken in 2016 semester.

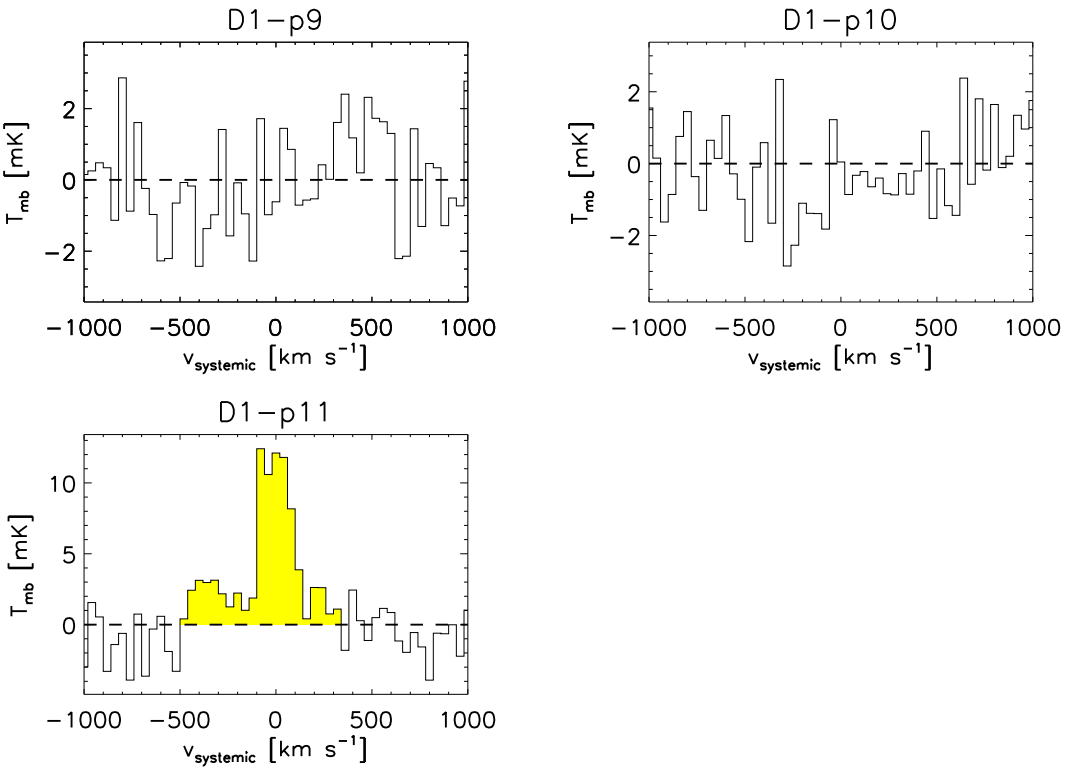

Figure 2.10: Continued from Figure 2.10.

Table 2.3: Summary of CO observation of our NRO 45m sample in 2015 semester.

Env.	I_{CO} [K km s^{-1}]	$\log L_{CO}$ [K km s^{-1}pc^2]	$\log M_{\rm H_2}$ [M$_\odot$]
D1-1	7.29± 0.27	9.36± 0.09	10.00± 0.09
D1-2	28.83± 1.27	9.48± 0.10	10.11± 0.10
D1-3	6.26± 0.40	9.63± 0.15	10.26± 0.15
D1-4	7.06± 0.45	9.23± 0.15	9.86± 0.15
D1-5	4.26± 0.35	9.31± 0.19	9.94± 0.19
D1-6	5.49± 0.40	9.60± 0.17	10.24± 0.17
D2-1	4.26± 0.31	8.82± 0.17	9.45± 0.17
D2-2	4.64± 0.31	9.32± 0.15	9.95± 0.15
D2-3	5.18± 0.59	9.42± 0.26	10.05± 0.26
D2-4	7.85± 0.69	9.56± 0.20	10.19± 0.20
D2-5	2.93± 0.35	9.06± 0.27	9.69± 0.27
D2-6	3.37± 0.39	9.36± 0.27	10.00± 0.27
D3-1	5.03± 0.32	9.36± 0.15	10.00± 0.15
D3-2	6.76± 0.67	9.08± 0.23	9.71± 0.23
D3-3	2.19± 0.28	9.31± 0.30	9.95± 0.30
D3-4	3.17± 0.43	8.67± 0.31	9.30± 0.31
D3-5	4.31± 0.52	9.26± 0.28	9.89± 0.28
D3-6	4.63± 0.37	9.29± 0.19	9.92± 0.18
D4-1	12.35± 0.54	10.32± 0.10	10.95± 0.10
D4-2	7.22± 0.47	9.53± 0.15	10.16± 0.15
D4-3	6.15± 0.32	9.31± 0.12	9.94± 0.12
D4-4	6.20± 0.32	9.24± 0.12	9.87± 0.12
D4-5	2.81± 0.37	9.45± 0.31	10.08± 0.31
D4-6	3.28± 0.42	9.14± 0.29	9.77± 0.29
D4-7	3.72± 0.47	9.91± 0.29	10.54± 0.29
D5-1	9.55± 0.57	9.61± 0.14	10.25± 0.14
D5-2	3.14± 0.41	8.76± 0.30	9.40± 0.30
D5-3	7.27± 0.43	9.73± 0.14	10.36± 0.14
D5-4	4.80± 0.25	9.15± 0.12	9.78± 0.12
D5-5	3.23± 0.29	9.16± 0.21	9.80± 0.20
D5-6	7.82± 0.71	9.29± 0.21	9.92± 0.21
D5-7	9.05± 0.49	9.34± 0.13	9.98± 0.13

IRAM 30m telescope for 366 galaxies in the redshift range of $0.025 < z < 0.05$.

Because the COLDGASS sample is drawn from SDSS, we can measure their local density in the same way as our sample. We note that the COLDGASS survey is not originally designed to cover a wide environmental range, and so it tends to lack galaxies in the high- and low-density environments (such as D1 or D5 in our definition). In addition, most of their samples are located on or below the MS relation, and the number of galaxies above the MS is limited. Our NRO 45m sample is therefore complementary to the COLDGASS sample with these respects.

We only use the COLDGASS sample with CO detection with $S/N > 5$, for 169 of which we have the local galaxy density measurement. We found that one target in our NRO 45m sample overlaps with one of the COLDGASS sample, and we confirmed that our CO intensity measurement is consistent with the COLDGASS measurement (with the IRAM 30m) within the error (typically 20 %) for this source.

2.5 Final Sample

By combining our new NRO 45m sample and the COLDGASS sample, our final sample includes 214 galaxies in total. The redshift range is $z = 0.025 - 0.16$. We note that there is a possibility that ρ_5 does not probe the physically same environment across this redshift range, because the stellar mass limit should be different for each redshift (particularly when the stellar mass distribution depends on the environment). In this study, we used all galaxies selected from a relatively wide redshift range to have a sufficiently large sample size across all environments, but we confirmed that our conclusions do not change even if we restrict the sample to those within a narrow redshift range (e.g. $z = 0.025 - 0.05$).

We calculate the molecular gas mass ($M_{\rm H_2}$) with $M_{\rm H_2} = \alpha_{\rm CO} L'_{\rm CO}$ adopting the Galactic value of $\alpha_{\rm CO}$ = 4.3 $M_\odot$ (K km s^{-1} pc^2)$^{-1}$, which includes the contribution of heavy elements (mainly from helium), as commonly used in studies of star-forming galaxies in the local universe (Bolatto et al., 2013). We use $\rm SFR_{SDSS}$ for all the galaxies, because it is not possible to estimate $\rm L_{IR}$ for galaxies with low SFR due to the detection limit of the *AKARI* FIR data. There may be a small systematic offset between $\rm SFR_{IR}$ and $\rm SFR_{SDSS}$ (by $\sim$0.3-dex level), as reported by some recent studies (e.g. Lee et al., 2013), but the results presented in this study based on *relative* comparison between different environments is not affected. As exception, we replace $\rm SFR_{SDSS}$s with the $\rm SFR_{IR}$s (see Table 2.1) regarding two of our (FIR-detected) NRO 45m targets. They show unrealistically small $\rm SFR_{SDSS}$s; their $\rm SFR_{SDSS}$s are two orders of magnitude smaller than $\rm SFR_{IR}$ because of the wrong SDSS fiber position. We note that our results do not change even if we exclude these two galaxies from our analysis.

Figure 2.11 shows the distribution of the final sample on the M_*–SFR plane in each environmental bin. As shown in this plot, the COLDGASS samples (diamonds) are distributed mainly below the MS relation, while our NRO galaxies (circles) are distributed on/above the MS relation (and below the MS relation for D1). The distribution of all the SDSS samples significantly changes with environment (see gray contours in each panel), but we stress again that the aim of this work is to cover a wide range in M_*, SFR, and environment, and to test the environmental dependence of galaxy properties at a fixed position on the M_*–SFR plane.

Table 2.4: Summary of CO observation of our NRO 45m sample in 2016 semester. Here, $COflag = 1$ means detection and 0 mean non-detection. For non-detection spectra, we estimate the 3σ upper limits.

Env.	I_{CO} [K km s^{-1}]	log L_{CO} [K km s^{-1}pc^2]	log $M_{\rm H_2}$ [M$_\odot$]	COflag
D1-p1	0.71± 0.36	8.23± 1.15	8.86± 0.22	1
D1-p2	0.93± 0.42	8.21± 1.04	8.85± 0.20	1
D1-p3	1.41± 0.51	8.47± 0.83	9.10± 0.16	1
D1-p4	1.01± 0.36	8.33± 0.82	8.96± 0.15	1
D1-p5	2.00± 0.35	8.78± 0.41	9.41± 0.08	1
D1-p6	1.11± 0.38	8.56± 0.79	9.19± 0.15	1
D1-p7	3.95± 0.59	9.11± 0.34	9.75± 0.07	1
D1-p8	1.73	8.54	9.17	0
D1-p9	1.65	8.53	9.16	0
D1-p10	1.31	8.44	9.07	0
D1-p11	3.48± 0.81	8.99± 0.54	9.63± 0.10	1

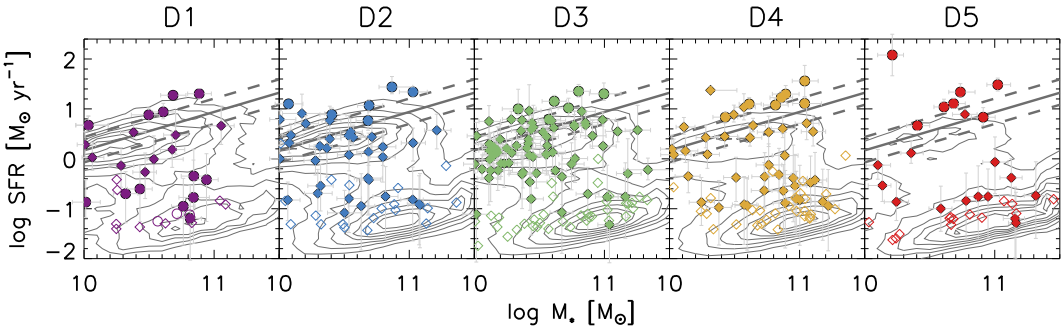

Figure 2.11: SFR–M$_*$ diagram for each environment (D1–D5). The circles show our NRO45m sample, and the diamonds show the sample from COLDGASS with CO detection, where filled and open symbols denote CO-detected and undetected sources, respectively. The solid line drawn in all the panels shows the main sequence relation in the local universe reported by Elbaz et al. (2007), and the broken lines show its 1-σ scatter. The gray contours show the distribution of all the SDSS sample for each environmental bin.

Chapter 3

Results

In this section, we investigate the relationship between star formation activity and molecular gas properties in different environments to reveal the environmental impacts on the molecular gas properties of galaxies (Section 3.1–3.2). We also study the influence of CO-undetected sources by performing stacking analysis on our results (Section 3.3). Furthermore, we discuss the effects of CO-to-H_2 conversion factor (Section 3.4) as well as the definition of environment on the results (Section 3.5).

3.1 M_{H_2}–SFR Relation

First, we investigate the environmental dependence of the correlation between M_{H_2} and SFR. This is the so-called global Kennicutt–Schmidt law, which is often recognized as one of the most fundamental star formation laws (Kennicitt, 1998). Figure 3.1 (top) shows the M_{H_2}–SFR relation for galaxies in each environmental bin. To compare the distribution in different environments, we first fit the data points in the D3 bin (i.e. the most "general" environment) by the liner regression form of $y = A + Bx$, where y is substituted by $\log SFR/M_\odot\ yr^{-1}$ and x is substituted by $\log M_{H_2}/M_\odot$, by using the Ordinary Least-Squares (OLS)–Bisector method. The gray dotted

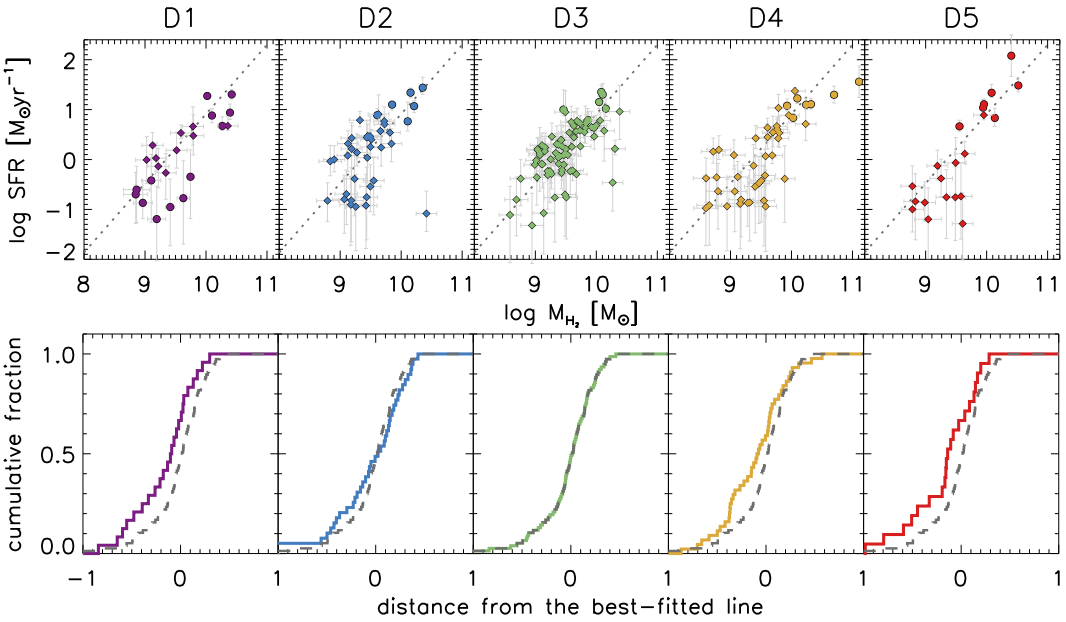

Figure 3.1: (top:) The relation between M_{H_2} and SFR for each environmental bin. For comparison, we show the best-fitting result for D3 bin with the gray dotted lines in all the panels. The meanings of the symbols are the same as Figure 2.11. (bottom:) The cumulative distribution functions of the distance from the best-fitted relation (defined for D3) for each environment (D1–D5). The solid line shows the cumulative function for each environmental bin, and the broken lines show that of D3 bin for comparison. Because we measure the distance from the best-fitted line defined for D3 sample, the solid line and broken lines are identical for D3 panel by definition.

Table 3.1: The p-values derived from the KS test for the residual distribution, where the residuals are defined as the orthogonal distances from the best-fitted line for D3 bin to each galaxy on the M_{H_2}–SFR, ΔMS–f_{H_2} and ΔMS–SFE planes.

	M_{H_2}–SFR	ΔMS–f_{H_2}	ΔMS–SFE
D1	0.20	0.09	0.25
D2	0.80	0.48	0.55
D3	1.00	1.00	1.00
D4	0.14	0.84	0.55
D5	0.07	0.93	0.75

line in each panel of Figure 3.1 (top) shows the best-fitting result for D3 bin. We then measure the distance in the orthogonal direction to this best-fitted line for each galaxy, and perform the two-sample Kolmogolov-Smirnov (KS) test between D1/D2/D4/D5 and D3 samples. The KS plots (the normalized cumulative distribution functions) are shown in Figure 3.1 (bottom), and the derived p-values, the probabilities that the D1/D2/D4/D5 and D3 samples are drawn from the same parent population, are summarized in Table 3.1. Their p-values are >0.05 in all cases, suggesting that we cannot rule out the hypothesis that M_{H_2}–SFR relations are universal across all environments. Therefore, we conclude that the M_{H_2}–SFR relation does not significantly depend on the environment.

3.2 f_{H_2} and SFE at fixed ΔMS

As mentioned in Section 1.2, it is reported that f_{H_2} and SFE are strongly correlated with ΔMS (Saintonge et al., 2012; Genzel et al., 2015; Saintonge et al., 2016). In this subsection, we study the ΔMS–f_{H_2} and ΔMS–SFE correlation for each environmental bin, to test the environmental dependence of the f_{H_2} and SFE at fixed ΔMS. Our aim here is to understand whether or not galaxies having the same star-formation activity, but existing in different environments, have the same amount of molecular gas and are forming stars with the same efficiency. It is well established that the MS relation changes with redshift, but there is no measurable change within the redshift range of our sample ($z = 0.025 - 0.16$) (Speagle et al., 2014). Furthermore, the MS relation does not significantly change with environment as reported by many recent studies (Peng et al., 2010; Koyama et al., 2013), and thus we simply define the ΔMS for all galaxies in our sample as the SFR offset value from the MS at $z = 0$:

$$\Delta\mathrm{MS} = \log SFR - \log SFR_{MS}, \tag{3.1}$$

where SFR_{MS} denotes the SFR of galaxies on the MS relation at a given M_*. We adopt the MS relation in the local universe defined by Elbaz et al. (2007) as follows:

$$\log SFR_{MS} = 0.77 \log M_* - 7.53, \tag{3.2}$$

as shown with the solid line in each panel of Figure 2.11. We note that our conclusions are unchanged even if we separately define the MS for each environment.

We show the ΔMS–$f_{\rm H_2}$ and the ΔMS–SFE correlation for each environmental bin (D1–D5) in Figure 3.2 and Figure 3.3, respectively. It can be seen that there exist strong ΔMS–$f_{\rm H_2}$ and ΔMS–SFE correlations in all environmental bins, and more importantly, there is no significant difference between different environments for both of the correlations. As we did in Figure 3.1, we first fit the data points in D3 bin by a linear regression form of $y = A + Bx$, where y is substituted by $\log f_{\rm H_2}$ (and $\log SFE$), and x is substituted by the ΔMS. We then perform the KS tests for the residual distributions as we did in the previous section, and we confirm that their p-values are >0.05 in all cases as summarized in Table 3.1, suggesting that we cannot rule out the hypothesis that all the environmental subsamples are drawn from the same parent population.

Overall, our results revealed that galaxies having the same star-formation activity (ΔMS), but existing in different environments, have the same amount of molecular gas and are forming stars with the same efficiency. This is the most important result of this study. The environmental independence of the ΔMS–$f_{\rm H_2}$ (or –SFE) correlations suggest that most galaxies are located on the same correlations with very few galaxies being scattered from the sequence. This implies that galaxies in all environments must evolve by moving along this sequence. More detailed discussion is provided in the next chapter.

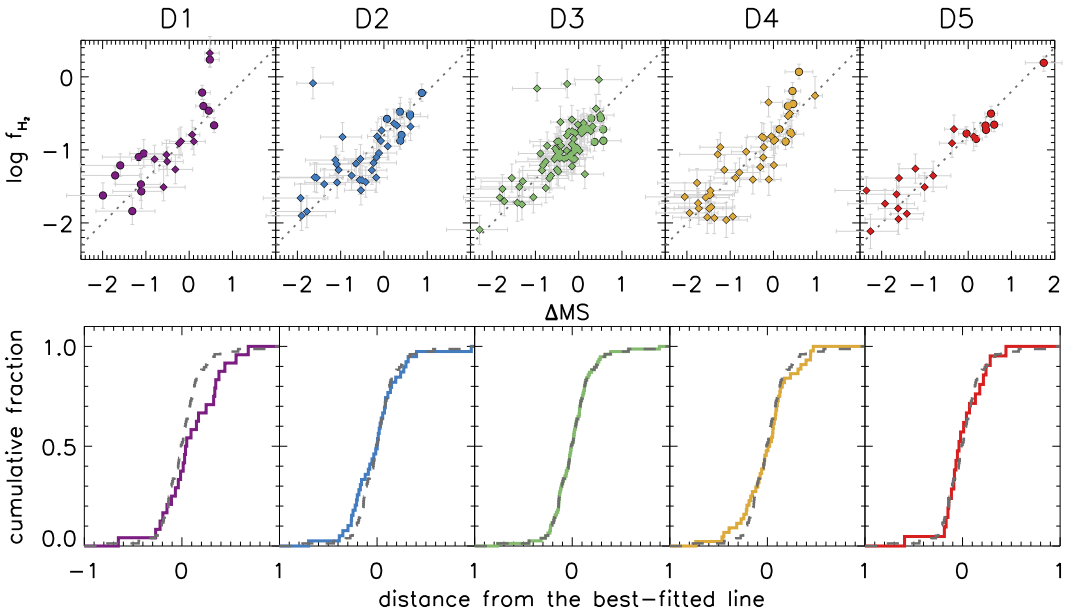

Figure 3.2: ΔMS–f_{H_2} relation for each environmental bin, and the cumulative distribution functions of the distance from the best-fitted relation (defined for D3) for each environment (D1–D5). The meanings of the color codings and symbol styles are the same as in Figure 3.1.

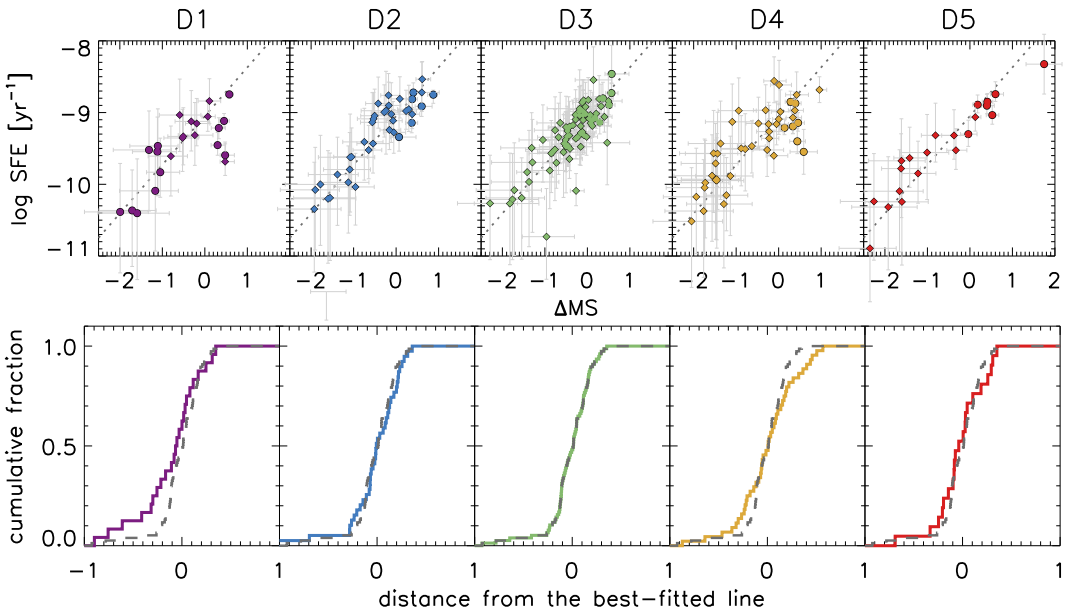

Figure 3.3: The same plots as Fig. 3.2 but for SFE. The meanings of the color coding and symbols are the same as in Figure 3.1 and Figure 3.2.

3.3 Stacking Analysis

The results shown in the previous sections are based on galaxies whose CO lines are individually detected. However, there exist some CO-undetected sources in our sample as well as in the COLDGASS sample, in particular for galaxies with low SFRs. In Figure 3.4, we show the ΔMS–$f_{\rm H_2}$ and – SFE correlations (same plots as Figure 3.2 and 3.3) by including all the CO-undetected sources with their 5σ upper limits. As shown in these figures, there exist a relatively large number of CO-undetected sources in the low ΔMS regime, indicating that we might overestimate the mean $f_{\rm H_2}$ and underestimate the mean SFE at the very low ΔMS region. It is therefore important to evaluate the influence of those CO-undetected sources on our results, to test if the $f_{\rm H_2}$ and SFE are dependent on the environment or not at the very low ΔMS regime.

For this purpose, we here apply the spectral stacking analysis, which is the commonly-used technique to obtain the mean spectrum and to derive the average galaxy properties for different subsamples of galaxies. By stacking the spectra, we can increase the signal to noise ratio (by reducing the $\rm T_{rms}$). Here, we stack the COLDGASS spectra of all galaxies regardless of their individual CO detection, with $\Delta{\rm MS} < -1$ for each environmental bin. We also stack all the spectra of the galaxies with $\Delta{\rm MS} < -1$ observed with NRO45m (for D1). Before stacking, we have to correct for the difference of redshift (distance) of each galaxy; otherwise the stacked spectrum will be more strongly affected by relatively low-z galaxies. We therefore scaled each spectrum S with the following equation:

$$S_{scaled} = \frac{SD_L^2}{(1+z)^3}, \tag{3.3}$$

where the factor $D_L^2/(1+z)^3$ is a term related to redshift in Eq. (2.4). We then get a stacked spectrum ($S_{stacked}$) by calculating the weighted mean of

S_{scaled}:

$$S_{stacked} = \frac{\Sigma_i w_i S_{scaled,i}}{\Sigma_i w_i}, \tag{3.4}$$

where w denotes $1/rms^2$ for each spectrum. We show the stacked spectra of COLDGASS sample for each environmental bin in Figure 3.5, and that of NRO45m sample for D1 environment in Figure 3.6. We thus successfully detected CO lines by stacking analysis for both NRO45m and COLDGASS sample, except for D1 sample in COLDGASS. We consider that non-detection of D1 sample in COLDGASS is due to small number of samples.

Then, we calculate their mean CO luminosities. Since the flux of COLDGASS spectra is given in the unit of Jy unlike NRO45m spectra, the equation to calculate the CO luminosity should be different from Eq. (2.4) (that we used for the NRO45m sample):

$$L'_{\rm CO} = \frac{3.25 \times 10^7 S_{\rm CO} D_L^2}{\nu_{obs}^2 (1+z)^3}, \tag{3.5}$$

where $L'_{\rm CO}$ is the CO luminosity in K km s^{-1} pc^2, $S_{\rm CO}$ is the integrated line flux in Jy km s^{-1}, ν_{obs} is the observed frequency of CO(1–0) lime in GHz, and D_L is the luminosity distance in Mpc. The spectra have already been multiplied by the term of $D_L^2/(1+z)^3$, and so we can calculate the CO luminosity by summing the flux within the velocity range colored in yellow in Figure 3.5 and 3.6, and multiplying the constant factors $3.25 \times 10^7 \nu_{obs}^{-2}$ for COLDGASS sample and Ω_b for NRO45m sample. Finally, $\rm M_{H_2}$ was calculated by multiplying the CO-to-$\rm H_2$ conversion factor $\alpha_{\rm CO} = 4.3\ \rm M_\odot\ (K\ km\,s^{-1}\,pc^2)^{-1}$.

In Figure 3.7, we show the relation between ΔMS and $f_{\rm H_2}$ (and SFE) for the stacked spectra. As shown in these figures, the differences between environmental bins are small and within the size of error-bars, although the "stacked" data points tend to be lower for $f_{\rm H_2}$ and higher for SFE, compared with the best-fitted line defined with "CO-detected" sources for D3. These results suggest that the CO-undetected sources have some impacts on the relation between star formation activity and molecular gas at the low ΔMS

region, but it does not depend on the environment. Therefore, we conclude that our conclusions are unchanged by the inclusion of the CO-undetected galaxies into our analysis.

3.4 CO-to-H_2 conversion factor

Throughout this study, we have assumed a conversion factor of $\alpha_{\rm CO}$=4.3 $M_\odot$ (K km s^{-1} pc^2)$^{-1}$ to convert L'_{co} into M_{H_2}. However, it is reported that gas temperature and gas surface density tend to increase in starburst galaxies (i.e. galaxies with high ΔMS), and their $\alpha_{\rm CO}$ tends to be lower than normal star-forming galaxies (e.g. Downes & Solomon, 1998). Because our galaxy samples have a wide variety of ΔMS, it is likely that $\alpha_{\rm CO}$ does not constant for all the galaxies we studied. It is also reported that $\alpha_{\rm CO}$ decreases with an increase of gas-phase metallicity (e.g. Bolatto et al., 2013). We show in Appendix A a possible environmental dependence of gas metallicity (at fixed stellar mass and ΔMS), suggesting that $\alpha_{\rm CO}$ should depend on the environment.

In this section, we examine how our results are affected if we apply the gas metallicity- and ΔMS-dependent $\alpha_{\rm CO}$. We here use the following equation recently established by Accurso et al. (2017) to describe $\alpha_{\rm CO}$ as a function of ΔMS and gas metallicity:

$$\log \alpha_{\rm CO} = 15.623 - 1.732[12 + \log({\rm O/H})] + 0.051 \log \Delta{\rm MS}. \quad (3.6)$$

Here, 12+log (O/H) is a unit of gas metallicity derived by O3N2 method (Pettini & Pagel, 2004):

$$12 + \log({\rm O/H}) = 8.73 - 0.32{\rm O3N2}, \quad (3.7)$$

where

$$\mathrm{O3N2} \equiv \log \frac{\frac{[\mathrm{OIII}]\lambda 5007}{\mathrm{H}\beta}}{\frac{[\mathrm{NII}]\lambda 6584}{\mathrm{H}\alpha}}. \quad (3.8)$$

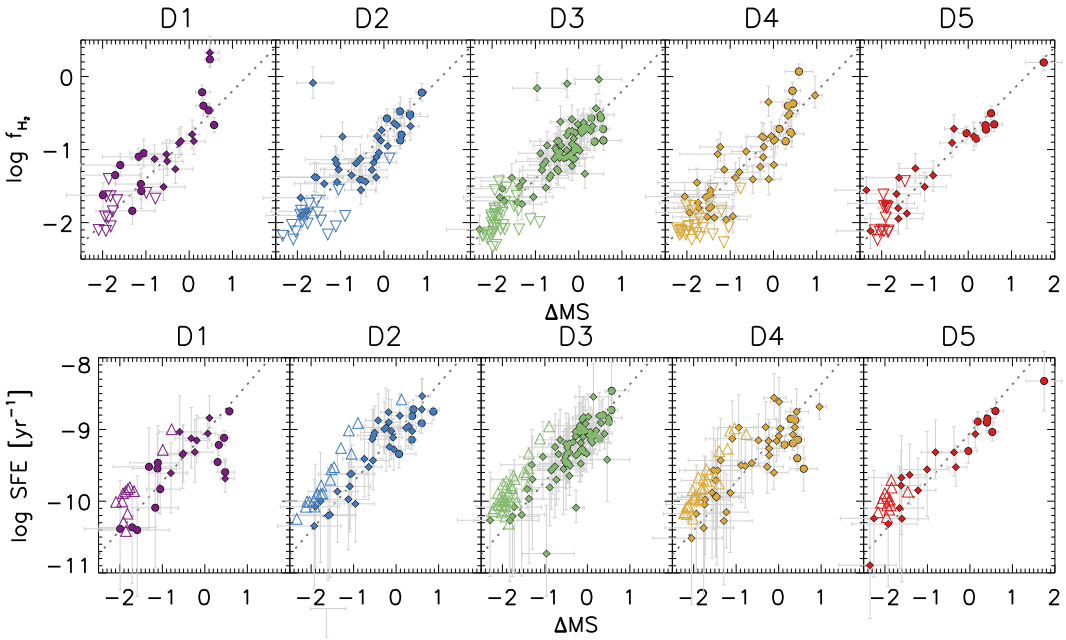

Figure 3.4: Same plot as Figure 3.2 and 3.3, but here we add the CO-undetected sources with the open triangles. Open downward and upward triangles show upper and lower limits, respectively.

Table 3.2: Summary of physical quantities of the stacked spectra.

Env.	log SFR [$M_\odot$ yr^{-1}]	log M_* [$M_\odot$]	log M_{H_2} [$M_\odot$]	COflag
		COLDGASS		
D1	-1.20± 0.09	10.64± 0.13	8.56	0
D2	-0.92± 0.06	10.69± 0.07	8.73± 0.23	1
D3	-1.03± 0.05	10.74± 0.06	8.47± 0.26	1
D4	-0.87± 0.05	10.84± 0.04	8.83± 0.15	1
D5	-1.03± 0.07	10.80± 0.08	8.91± 0.15	1
		NRO45m		
D1	-0.84± 0.09	10.64± 0.08	9.19± 0.15	1

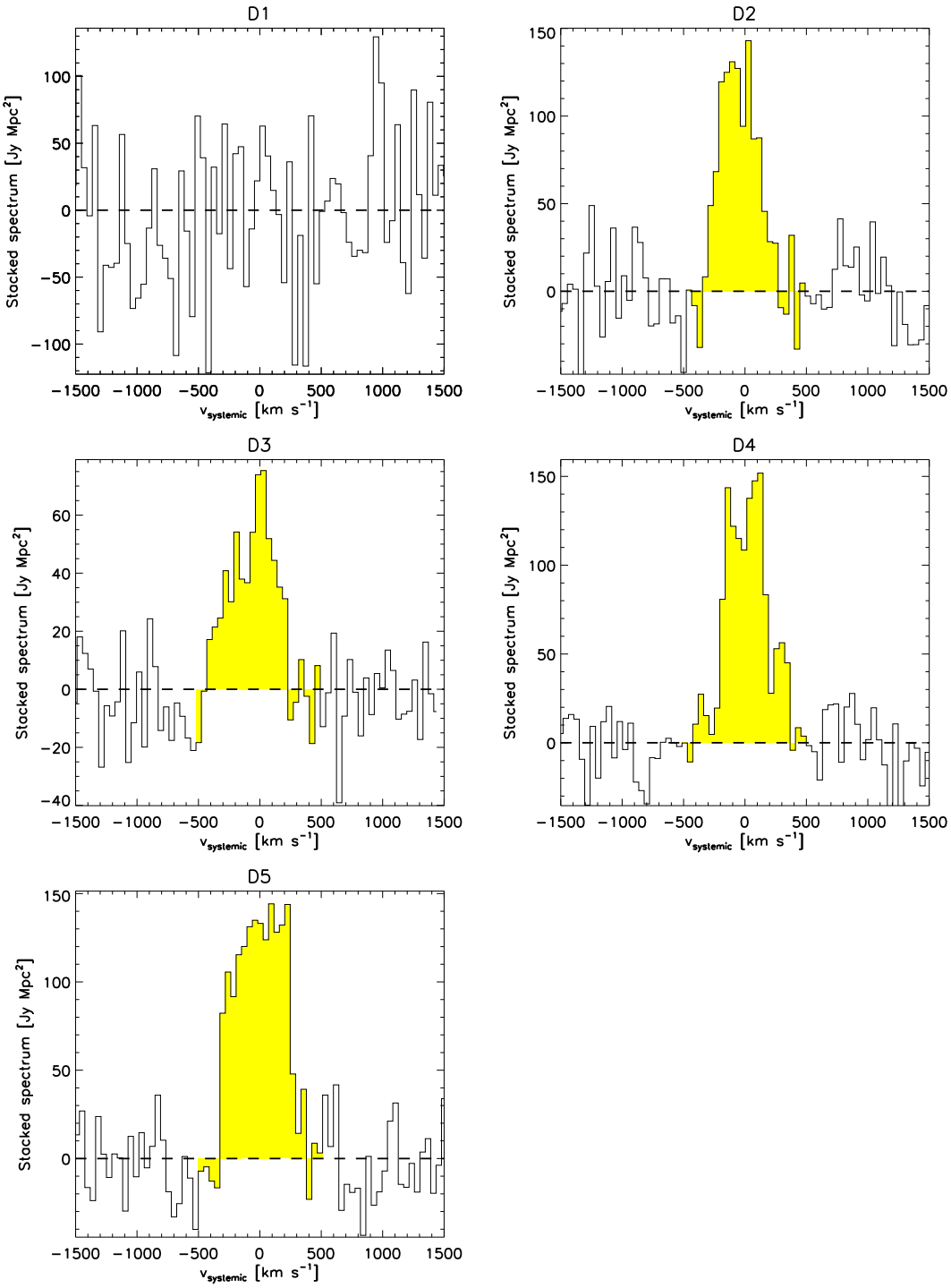

Figure 3.5: The stacked CO spectra for COLDGASS sample with ΔMS < -1 for each environmental bin.

On the other hand, gas metallicity listed in the MPA-JHU catalog is calculated by Tremonti et al. (2004, T04) method, which derives the gas metallicity by fitting a theoretical model to the strong emission lines of galaxies such as [OII], Hβ, [OIII], Hα, [NII] and [SII]. We therefore convert the gas metallicity (T04) into O3N2 using the conversion formula provided by Kewley & Ellison (2008):

$$y = 230.7820 - 75.79752x + 8.526986x^2 - 0.3162894x^3, \qquad (3.9)$$

where $x = 12 + \log(\mathrm{O/H})_{\mathrm{T04}}$ and $y = 12 + \log(\mathrm{O/H})_{\mathrm{O3N2}}$. Using these equations, we find that our galaxy sample has $\alpha_{CO} = 1.5$ – 7.4, according to the ranges of gas metallicity and ΔMS with $12 + \log(\mathrm{O/H})_{\mathrm{O3N2}} = 8.5$ – 8.9 and ΔMS = -1.4 – 1.7.

We update the α_{CO} (hence M_{H_2}) for individual galaxies following the above equation, and we plot in Figure 3.8 the updated version of the ΔMS–f_{H_2} and –SFE relations. Because the gas-phase metallicity is calculated by the optical line flux ratio, it is not possible to calculate the gas metallicity for galaxies with low star formation activity. In Figure 3.8, we plot galaxies for which we can successfully calculate gas metallicity.

It can be seen that the correlations are still universal across environments, and the p-values from the KS test are also consistent with our results under the assumption of constant α_{CO} except D1 (Table 3.3), where the sample size is very small at the low ΔMS end. We therefore conclude that applying the variable CO-to-H_2 conversion factor does not affect our results on the environmental independence of the ΔMS–f_{H_2} and –SFE correlations.

3.5 Local number density vs. halo mass

As described in Section 2.2, we utilize the local number density of galaxies to quantify the environment. The local number density is an environmental

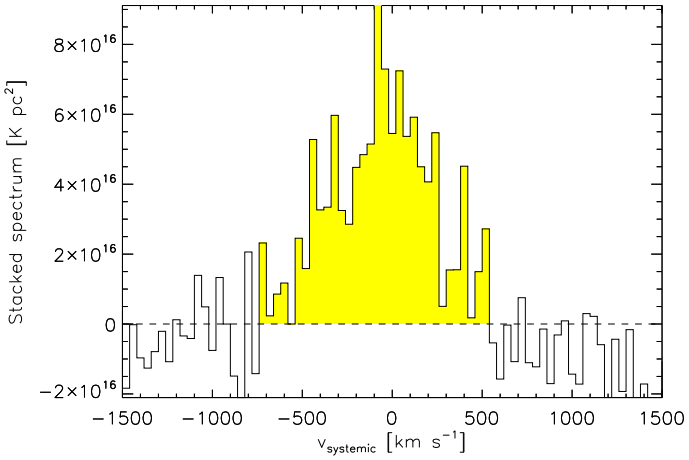

Figure 3.6: The stacked CO spectrum for NRO45m sample with ΔMS $< -1 for D1 bin$.

Table 3.3: The p-values for Figure 3.8.

	ΔMS–$f_{\mathrm{H_2}}$	ΔMS–SFE
D1	0.03	0.001
D2	0.84	0.49
D3	1.00	1.00
D4	0.71	0.10
D5	0.08	0.10

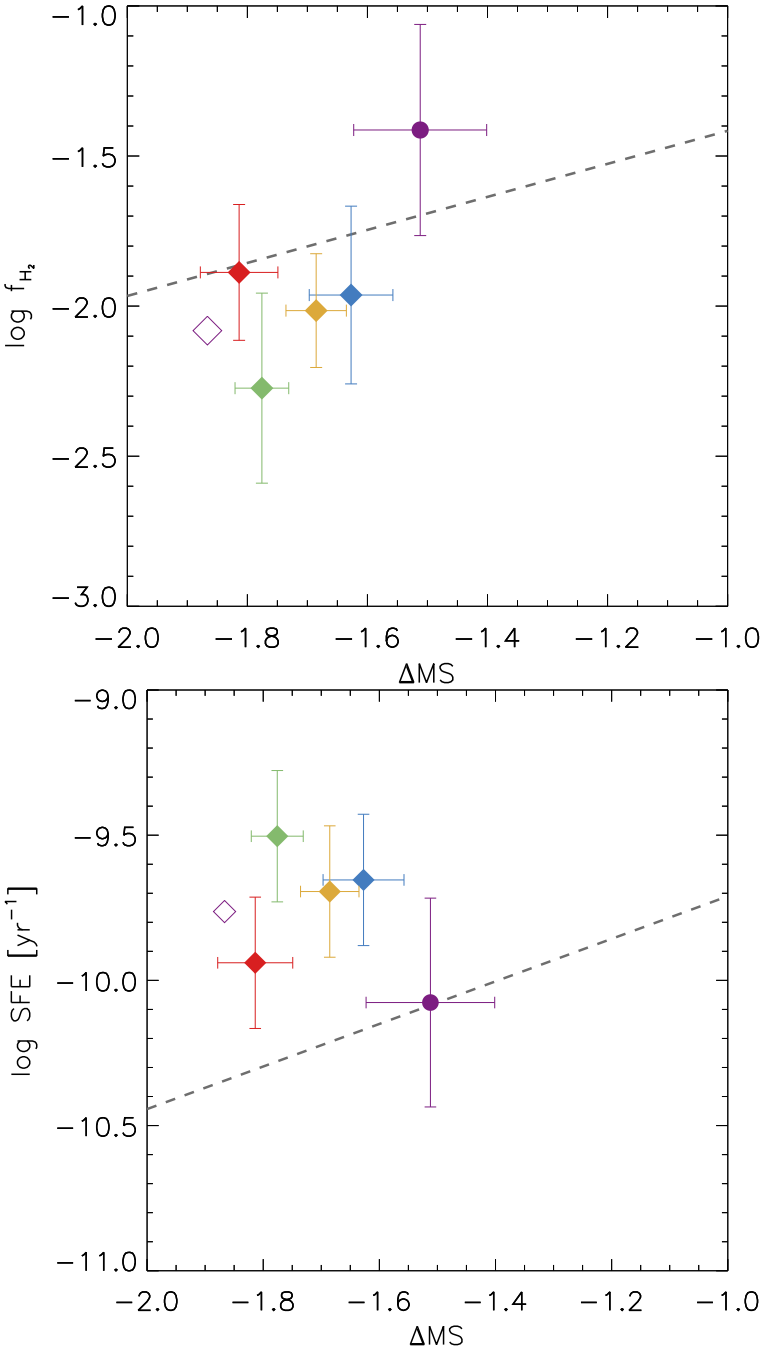

Figure 3.7: The relation between ΔMS and $f_{\mathrm{H_2}}$ (and –SFE) of stacked data for each environmental bin. The color coding follows previous figures. Circles show the NRO45m data, and diamonds show the COLDGASS data. Open symbol means non-detection.

definition commonly used by many studies, while there is another common definition of environment—the halo mass (M_h). Dark matter halo is a galaxy component that envelops the visible regions of galaxies, and dominates total galaxy mass. Because it is well known that member galaxies in galaxy groups or clusters share the same (massive) halo, and that their total stellar mass is tightly correlated with M_h (Yang et al., 2007), M_h is another useful, quantitative measure for the environmental definition. In this subsection, we investigate how our results are affected (or unaffected) by the definition of environment, by repeating the same analyses using the M_h instead of the local density (ρ_5).

We utilize the SDSS group catalog (Yang et al., 2007), which assigns M_h for all galaxies in the SDSS catalog. They have determined M_h by using correlation between group stellar mass and M_h. In Figure 3.9, we show the relation between ρ_5 and M_h. These two quantities are weakly correlated with each other at $\rho_5 > 0$, while there seems to be no correlation at $\rho_5 < 0$. This suggests that ρ_5 and M_h do not necessarily trace the same environment; i.e. galaxies associated to more massive halo tend to reside in higher-density environment, while it is not always true for those in lower mass halo.

In Figure 3.10, we show how the red galaxy fraction ($= N(\Delta\mathrm{MS} < -1)/N(total)$) changes on the ρ_5–M_h plane. As shown in this figure, the red fraction is more strongly dependent on ρ_5 than M_h, but at $\rho_5 > 0$, M_h also significantly affects the red fraction at fixed ρ_5. We suggest that the star formation activity of galaxies mainly depends on ρ_5, while it also depends on M_h independently. Thus, it is worth investigating the dependence of the ΔMS–$f_{\mathrm{H_2}}$ and –SFE correlations on M_h. We here divide the sample into three M_h bins based on the following criteria: $\log M_h/M_\odot < 12.5$, $12.5 < \log M_h/M_\odot < 13.5$, $13.5 < \log M_h/M_\odot$. The ΔMS–$f_{\mathrm{H_2}}$ and –SFE correlations for three subsamples are shown in Figure 3.11. The gray dotted line in each panel shows the best-fitting result for $12.5 < \log M_h/M_\odot < 13.5$ bin. It can be seen that there

exist strong ΔMS–$f_{\rm H_2}$ and ΔMS–SFE correlations in all M_h bins, and there is no significant difference between different M_h bins. We also measure the distance in the orthogonal direction to this best-fitted line for each galaxy, and then perform the KS tests and confirm that their p-values are >0.05 in all cases (Table 3.4). We therefore conclude that the ΔMS–f_{H_2} and –SFE correlations are also universal across M_h, same as our results obtained by using the local number density.

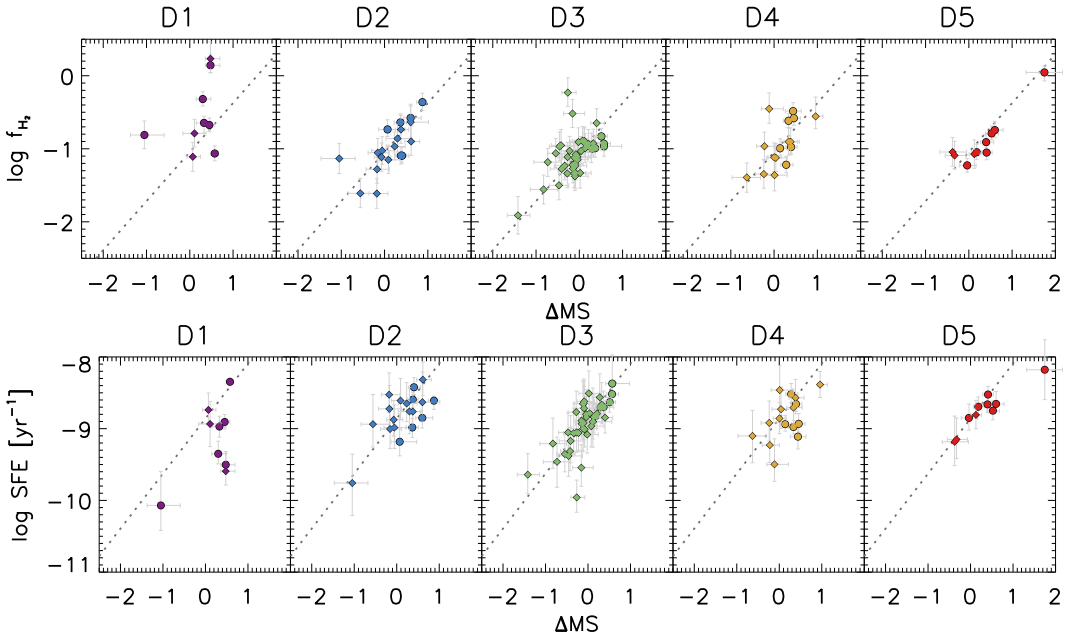

Figure 3.8: Same plots as Figure 3.2 and 3.3 in the case we apply the non-universal $\alpha_{\rm CO}$ (see Eq. 3.6).

Table 3.4: The p-values for Figure 3.11.

	ΔMS–$f_{\rm H_2}$	ΔMS–SFE
$M_h < 12.5$	00.11	0.53
$12.5 < M_h < 13.5$	1.00	1.00
$13.5 < M_h$	0.50	0.99

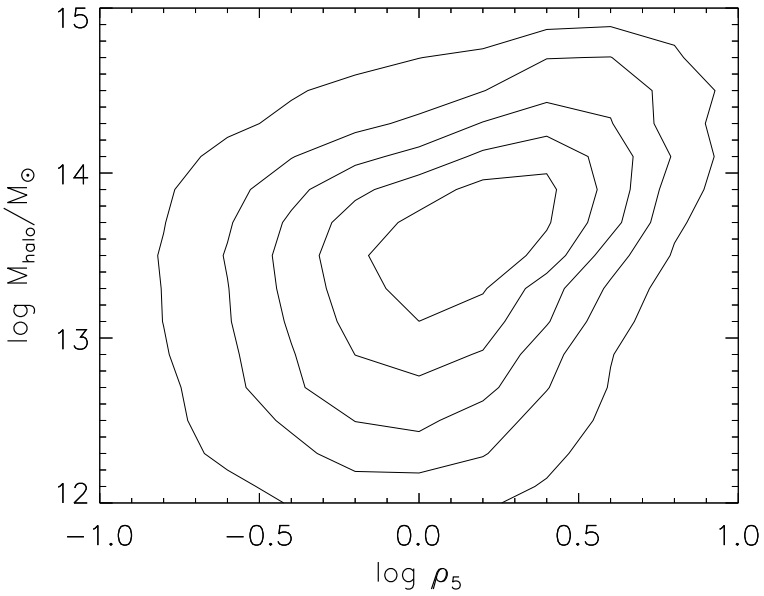

Figure 3.9: This contour shows the distribution of all the SDSS galaxies on ρ_5–M_h plane.

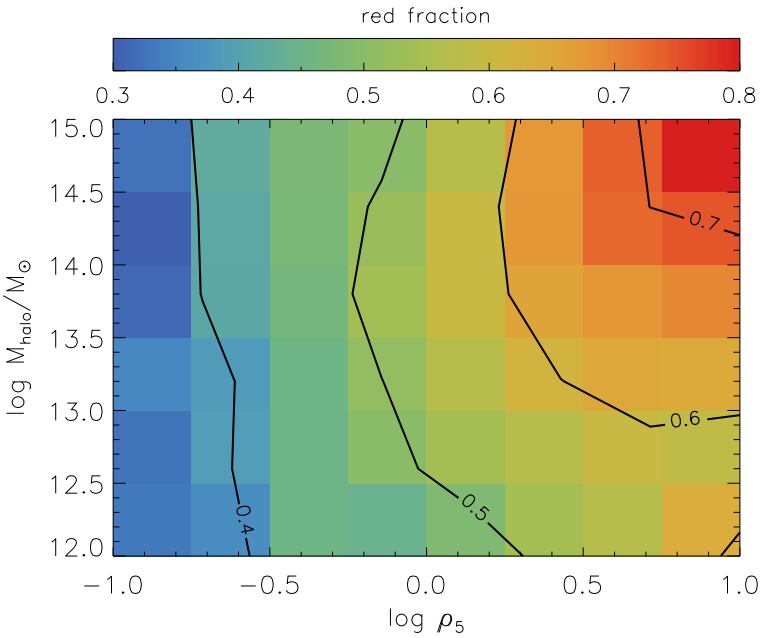

Figure 3.10: The distribution of red fraction($= N(\Delta\mathrm{MS} < -1)/N(total)$) on ρ_5–M_h plane.

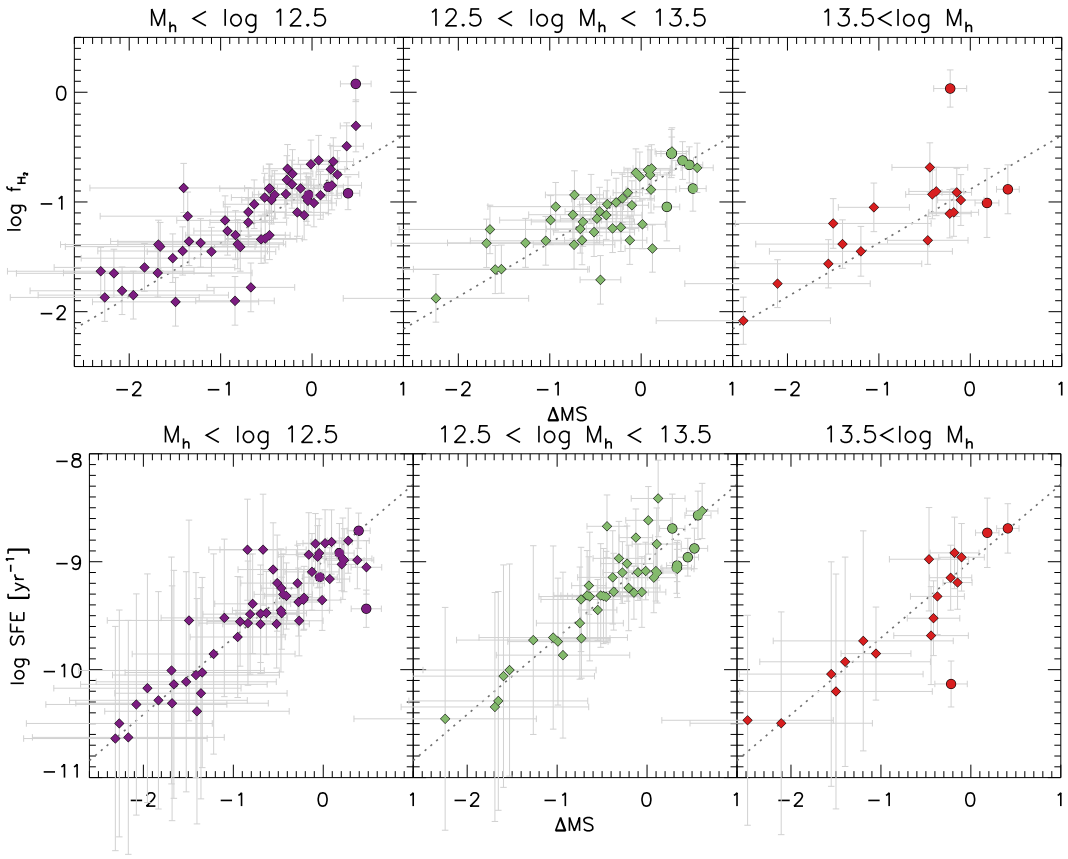

Figure 3.11: ΔMS–$f_{\mathrm{H_2}}$ (and –SFE) correlations for each halo mass bin. Gray dotted lines in all panels are the best-fitting result for the subsample of $12.5 < \log M_h < 13.5$.

Chapter 4

Discussion

The aim of this thesis is to reveal why galaxy quenching is accelerated in high-density environment by investigating their molecular gas properties. We have now found from our analyses that the environment does not affect the ΔMS–$f_{\rm H_2}$ (and –SFE) correlations, suggesting that galaxies having the same star-formation activity, but existing in different environments, have the same amount of molecular gas and are forming stars with the same efficiency.

In this chapter, we first provide an interpretation of our results by comparing our work with previous studies discussing environmental impacts on molecular gas (Section 4.1), and then we discuss which mechanism(s) is(are) reasonable for the environmental effects (Section 4.2).

4.1 Comparison with Previous Studies

As we mentioned in Section 1.2, many studies have investigated the environmental effects on the molecular gas content in various types of galaxies using CO observations. For example, Kenney & Young (1989), Casoli et al. (1991) and Lavezzi & Dickey (1998) performed CO observations of nearby cluster galaxies selected with B-band or far-IR luminosities. These studies suggest that the molecular gas content ($f_{\rm H_2}$) in galaxies is the same for cluster and isolated galaxies, but it should be noted that the B-band and far-IR selections are sensitive to the current/recent star formation, so that their samples tend to be biased to actively star-forming galaxies. On the other hand, more recent studies by Fumagalli & Gavazzi (2008), Scott et al. (2013) and Boselli et al. (2014) showed that cluster galaxies tend to have *lower* molecular gas mass fraction on average than isolated galaxies. Their galaxy samples are optically selected, which is less biased to recent star formation.

In our current work, we demonstrated that the $f_{\rm H_2}$ is constant at fixed ΔMS in all environments, suggesting that the average $f_{\rm H_2}$ of each environmental subsample should be determined by the average ΔMS of the sample. Because the original ΔMS distribution for *all* galaxies is shown to be significantly dependent on environment (see Figure 2.2), it is not surprising to see the trend that $f_{\rm H_2}$ and SFE tend to be lower in higher-density environments, if the galaxies are selected randomly from each environment without considering their ΔMS distribution. We therefore expect that the apparently different suggestions made by different authors regarding the environmental impacts on the molecular gas content in galaxies can be originated by their different sample selection. We emphasize again that our results may leave an important message for all studies discussing the environmental effects on the molecular gas content in galaxies; i.e. one always needs to be careful about how they select the sample when investigating the environmental effects on

the molecular gas content in galaxies.

We also comment that, although we attempted to cover as wide environmental range as possible, our sample may not fully cover the highest-density rich cluster environment. Our "D5" environment, the highest-density environment in our study, seems to correspond to a relatively wide environmental range from clusters to the filamentary structures (as demonstrated in Figure 2.3). Recent studies by Mok et al. (2016, 2017) demonstrate that the spiral galaxies in the Virgo cluster have *larger* amount of M_{H_2} and *longer* gas depletion time (M_{H_2}/SFR) than field/group galaxies, claiming that the cluster environment affects the efficiency of star formation through molecular gas heating or turbulence. On the other hand, some studies suggest that ram pressure in rich cluster environments compresses the gas in galaxies, and can enhance the star formation in the cluster member galaxies (e.g. Ebeling et al., 2014; Lee et al., 2017). In these ways, the effect of rich cluster environments on molecular gas content in galaxies is still under debate, but it is possible that galaxies in extremely rich environments could deviate from the ΔMS–f_{H_2} (or ΔMS–SFE) relations. A more comprehensive study, which hopefully covers a wider environmental range with larger samples from the lowest- to highest-density environments, is needed to fully understand the effect of such extreme environments.

4.2 Implication for Environmental Effect

4.2.1 Interpretation of the Universal Correlations

In this thesis, we have reported that ΔMS is tightly correlated with both $f_{\rm H_2}$ and SFE, and these correlations are universal across environments. In addition, by remembering the fact that the distribution of ΔMS significantly changes with environment in the sense that average ΔMS is lower for galaxies in higher-density environments (Figure 2.2), we expect that $f_{\rm H_2}$ and SFE should decrease with increasing environmental density following the ΔMS–$f_{\rm H_2}$ and –SFE correlations. Because the star formation activity (ΔMS) is primarily controlled by the molecular gas, it is expected that the role of environment is to reduce the molecular gas reservoir in galaxies.

We therefore suggest that there must be some environmental mechanisms which reduce the molecular gas reservoir without violating the ΔMS–f_{H_2} (and –SFE) correlations. In other words, when a galaxy loses a fraction of its molecular gas content due to some environmental effects, the star formation activity (ΔMS) needs to be "adjusted" accordingly in relatively short time-scale to come back onto the original ΔMS–$f_{\rm H_2}$ (and –SFE) correlations. We can expect that this time-scale is comparable to that of star formation (τ_{sf}) which is typically $\sim 10^{7-8}$ yr (e.g. Egusa et al., 2009). Accordingly, we suggest that the mechanism(s) responsible for the environmental effects have to reduce the molecular gas reservoir in longer time-scale than τ_{sf}.

4.2.2 Possible Mechanisms

The final question to be addressed in this thesis is: what is the most plausible mechanism responsible for the environmental effect? As we described above, our requirement is that the time-scale for the removal/consumption

of molecular gas ($\tau_{\mathrm{H_2}\,lose}$) must be longer than that of star formation:

$$\tau_{\mathrm{H_2}\,lose} > \tau_{sf} \approx 10^{7-8}\,\mathrm{yr}. \tag{4.1}$$

Because typical time-scales ($\tau_{\mathrm{H_2}\,lose}$) for the gas removal/consumption are known to be different for different physical mechanisms, we can infer the possible mechanisms with this approach. Here, we divide the mechanisms into two major categories: (1) molecular gas stripping and (2) suppression of molecular gas supply. We briefly describe below the two processes as well as their supporting evidence from the literature, and discuss which mechanism satisfies our requirement of gas-losing time-scale.

Molecular gas stripping

Molecular gas stripping is the most direct process to reduce the molecular gas reservoir of galaxies. Theoretically, it is considered that molecular gas can be stripped by ram pressure from IGM (Gunn & Gott, 1972), galaxy-galaxy interaction such as tidal stripping and galaxy harassment (Spitzer & Baade, 1951; Moore et al., 1996). In the case of ram pressure stripping, simulations suggest that $\tau_{\mathrm{H_2}\,lose}$ would be very short (order of $\sim 10^7\,\mathrm{yr}$) for a rich cluster such as Coma (Abadi et al., 1999). On the other hand, the time-scale of galaxy-galaxy interaction is expected to be $\sim 10^9\,\mathrm{yr}$. It seems to meet the requirements, however it can also be induced the short-lived ($\sim 10^8\,\mathrm{yr}$) starburst by gas compression simultaneously (Hopkins & Hernquist, 2010), which should make outliers on ΔMS–$f_{\mathrm{H_2}}$ (and –SFE) correlations by increasing SFE in high-density environment. In these ways, since both mechanisms have shorter time-scale than τ_{sf}, we here conclude that these are not a dominant mechanisms for the environmental effects.

Suppression of molecular gas supply

As described in Section 1.2, many studies proposed that the amount of atomic gas is decreased for star-forming galaxies in cluster environment (Giovanelli & Hynes, 1985; Chung et al., 2009; Cortese et al., 2011; Serra et al., 2012), as well as in group environment (Kilborn et al., 2009; Rasmussen et al., 2012; Catinella et al., 2013; Brown et al., 2017). Since the atomic gas is a fuel for the molecular gas, it is expected that the deficit of atomic gas can cause a suppression of molecular gas supply. If the molecular gas supply is halted, galaxies cannot replenish the molecular gas consumed by star formation any more, and will eventually shut down their star formation.

We expect that the mechanism responsible for the depletion of atomic gas would be similar to that of molecular gas stripping described above. However, since the atomic gas is widely distributed over the galaxy (and is less strongly bound to the gravitational potential of the galaxy), the atomic gas component can more easily be stripped than the molecular gas. Furthermore, atomic gas is also depleted by the so-called "strangulation" mechanism (Larson et al., 1980; Peng et al., 2015). Atomic gas in galaxies is supplied from the gas surrounding the galaxies (i.e. circumgalactic medium; CGM), which is the source of gas inflow (e.g. Jason et al., 2016). Since CGM can be stripped or heated in high-density environments (or in massive halos), atomic gas supply onto galaxies from CGM can be suppressed. Some observational studies support this mechanism at work in high-density environment (e.g. Maier et al., 2016; van de Voort et al., 2017).

It is suggested that the time-scale of strangulation is an order of $\sim 10^9\,\mathrm{yr}$ (Peng et al., 2015), which is much longer than that of e.g. ram pressure stripping. We note that, unlike the molecular gas stripping, the time-scale of the molecular gas depletion by these mechanisms would be determined by the time-scale of HI-to-H_2 conversion. Since there is no significant correlation

between atomic gas and star formation (Jaskot et al., 2015), it is expected that the typical time-scale of HI-to-H_2 transformation should be longer than τ_{sf}. We therefore conclude that some "milder" processes such as strangulation (or atomic gas removal) which indirectly suppress the molecular gas supply would be more preferable than the more violent mechanisms which directly strip the molecular gas content from the galaxies.

Chapter 5

Summary

5.1 Summary of This Thesis

In this thesis, we present the environmental effects on the molecular gas mass fraction ($f_{\rm H_2}$) and star-formation efficiency (SFE) of local galaxies, based on our new CO(1–0) observation at the NRO 45m telescope and the data from COLDGASS survey. Our final CO(1–0) sample covers a wide stellar mass and SFR range, and also covers a wide environmental range over two orders of magnitudes in the local number density of galaxies measured with SDSS DR7 spectroscopic galaxy sample. Our findings are summarized as follows.

- The correlation between $\rm M_{H_2}$ and SFR, the so-called "integrated Kennicutt-Schmidt law", does not significantly depend on their surrounding environment; i.e. the star-formation law is universal across environments (Section 3.1).

- Both $f_{\rm H_2}$ and SFE show strong positive correlations with the SFR offset from the star-forming main sequence (ΔMS), consistent with recent studies. These correlations are universal across all environments (Section 3.2), suggesting that galaxies having the same star-formation activity (ΔMS), but existing in different environments, have the same

amount of molecular gas and are forming stars with the same efficiency.

- We carefully examined possible biases and systematics which might affect our conclusion on the environmental independence of ΔMS–$f_{\rm H_2}$ and –SFE correlations as the following:

  1) There exist some CO-undetected sources both in our NRO45m sample and in the COLDGASS sample, in particular at the low SFR regime. Those CO-undetected sources are not used in our main analyses. To evaluate the effect of such CO-undetected sources (and with a hope to extend the universal correlations down to the low ΔMS range), we applied a spectral stacking analysis and revealed that the universal correlations can be extended to low ΔMS end and that our results are unchanged even if we include those CO-undetected galaxies into analysis (Section 3.3).

  2) While we adopted the constant CO-to-H_2 conversion factor ($\alpha_{\rm CO} = 4.3$) throughout our main analyses, some recent studies suggest that $\alpha_{\rm CO}$ depends on gas metallicity and ΔMS. Because our samples are distributed in a wide ΔMS coverage, and there is a hint that the gas-phase metallicity depends on the environment (Appendix A), we repeated our analysis using the gas metallicity- and ΔMS-dependent $\alpha_{\rm CO}$, and confirmed that applying the updated $\alpha_{\rm CO}$ does not affect our results on the environmental independence of the ΔMS–f_{H_2} and –SFE correlations (Section 3.4).

  3) We also investigate how our results are affected in the case we use another commonly-used definition of environment, halo mass (M_h), instead of the local number density. As expected, we showed that star formation activity depends on M_h, and we investigated the dependence of the ΔMS–$f_{\rm H_2}$ and –SFE correlations on M_h. We find that the correlations are universal across M_h, consistent with our results obtained

by using the local number density (Section 3.5).

- The environmentally independent ΔMS–$f_{\rm H_2}$ correlation revealed in this study leaves an important message for all studies discussing environmental impacts on the molecular gas properties in galaxies. We emphasize that the sample selection, more specifically the ΔMS distribution of the samples, is critically important for any environmental studies focusing on the H_2 gas in galaxies. To perform a fair comparison between the samples drawn from different environments, the sample should be carefully selected so that there is no bias in the ΔMS range between the samples (Section 4.1).

- Our findings suggest that the star formation process occurring within individual galaxies is not strongly affected by their global environment, but primarily controlled by their molecular gas content, and thus the role of environment is to reduce the gas reservoir in galaxies. Since tight ΔMS–$f_{\rm H_2}$ (and –SFE) correlations indicate that the mechanism(s) responsible for the environmental effects must reduce the molecular gas in longer time-scale than that of star formation. Following this requirement, we infer that the suppression of molecular gas supply through atomic gas stripping or strangulation would be the most plausible mechanism responsible for the environmental effects (Section 4.2).

5.2 Future Prospects

We revealed a universal correlation between molecular gas properties and star formation activity across environment, and according to the results, we suggest that the most plausible mechanism of the environmental effect is the strangulation. We note that, in addition to firmly conclude our proposed scenario, we need to get additional information to identify the key mechanism responsible for the environmental effects on molecular gas in galaxies. Here

are three examples of my research plans as future prospects.

5.2.1 Extend to Low Mass Galaxies

In this thesis, we focused on the environmental impacts on the molecular gas content within relatively massive galaxies with $\log M_*/\mathrm{M}_\odot > 10$. We had to apply this stellar mass cut because of the limited sensitivity and sample size of the currently available dataset including our own data taken with NRO45m telescope. However, it is reported that the environmental effects could more strongly affect low-mass galaxies than high-mass galaxies (Peng et al., 2010). Therefore, we consider that extending our CO(1–0) observations to lower-mass galaxies is one of the important next steps. Fortunately, there was a recent release of xCOLDGASS (Saintonge et al., 2017) catalog, which includes the CO(1–0) spectra of galaxies down to $\log M_*/\mathrm{M}_\odot = 9$. By making use of this newly released CO(1–0) data as the control sample of low-mass field galaxies, we can investigate the environmental impacts on molecular gas in low-mass galaxies by observing CO lines of those in very high- and very low-density environments—this is exactly the same approach we took in this thesis for massive galaxies.

5.2.2 Spatially Resolved Observation

It is also interesting to spatially resolve the molecular gas distribution within individual galaxies, because the molecular gas distribution may be changed by the environmental effects. The distribution of molecular gas content within the galaxies will provide us with a key insight on the environmental mechanism at work, because it is expected that different mechanism (e.g. ram pressure/tidal stripping or strangulation) have different impacts on the distribution of gas content within the galaxies. As described in Section 4.2, if ram pressure/tidal stripping is the main driver for gas removal, gas in the

outer regions of galaxies should be preferentially stripped, while if strangulation is at work, gas supply onto the galaxies should be uniformly suppressed.

Spatially resolved molecular gas mapping within galaxies can be made by observations with long-baseline interferometers such as the Atacama Large Millimeter/submillimeter Array (ALMA). We believe that the CO(1–0) galaxy samples used in this thesis covering a wide environmental range will provide excellent targets for future ALMA observations to reveal the mechanism of the environmental effects.

5.2.3 Extend to High-z Universe

It is also of great interests to extend our study in the local universe toward the high-z universe. It is demonstrated that the star formation activity in cluster environment (defined as the cluster total star formation rate normalized by cluster mass) increases dramatically with redshift following $(1 + z)^6$ from $z = 0$ to 2.5 (Shimakawa et al., 2014), suggesting that the environmental quenching should take place in such high-z universe. Therefore, I consider that it is very important to reveal the relation between star formation activity and molecular gas across wide environmental range in the distant universe, and to reveal the early phase of environmental quenching process.

Appendix A

Gas metallicity

Gas-phase metallicity (Z_{gas}) of galaxies represents a metal (any element heavier than He) abundance in their gas component as follows:

$$Z_{gas} = M_{metal}/M_{gas}, \tag{A.1}$$

and is generally described by the relative composition of hydrogen and oxygen as $12 + \log(\mathrm{O/H})$. Using the gas metallicity listed in the MPA-JHU catalog calculated by Tremonti et al. (2004), we here check the environmental dependence of gas metallicity in galaxies. In addition to its possible influence on the CO-to-H_2 conversion factor that we used in this thesis (see Section 3.4), understanding the environmental dependence/independence of the gas metallicity of galaxies can provide us with a key insight into the physical mechanism(s) responsible for the environmental effects.

It is well known that there is a correlation between the gas metallicity and stellar mass of galaxies, so called "mass–metallicity relation" (MZR; Tremonti et al., 2004). Since most of the metals are formed in stars, metallicity of galaxies is expected to increase with stellar mass because stellar mass reflects the amount of stars formed in the past (or in other words, integrated star formation history). It should also be noted that the metallicity of galaxies can also be influenced by galactic-scale inflow and/or outflow pro-

cess. If there is a metal-poor gas supply (inflow) from the outer galaxy, it would 'dilute' the total metal abundance within the galaxy, and decrease its gas metallicity. In addition, if there is an outflow of gas from the galaxy via e.g. energetic or momentum-driven winds, it can eject the gas and metals from the galaxy, and its gas metallicity can also be decreased. In these ways, the gas-phase metallicity of galaxies can be regulated by the balance between chemical enrichment by star formation within the galaxies and their gas inflow/outflow processes.

In Figure A.1, we show the MZRs for our SDSS sample with the redshift range of $0.025 < z < 0.16$ by dividing them into three ΔMS bins. The left-, middle-, and right-panels show the results for those located in the upper-side envelop of the MS ($0.0 < \Delta\mathrm{MS} < 0.3$), lower-side envelop of the MS ($-0.3 < \Delta\mathrm{MS} < 0.0$), and for green-valley galaxies ($-0.3 < \Delta\mathrm{MS} < -0.6$), respectively. In each plot, we further split the sample into five environmental bins (D1–D5), and they are shown with different colors. The data suggest that the gas metallicity does not significantly change with environment for galaxies on the SFMS, while it can be seen that the gas metallicity of galaxies in higher-density environment tend to be higher at fixed stellar mass for the green-valley galaxies (right panel). This result implies that there are some environmental impacts on the gas-phase metallicity of galaxies in their "quenching phase". Although more detailed modeling would be required to further constrain the physical driver of the environmental dependence of MZR for galaxies in quehcnihg phase, we expect that the result might be related to the suppression of gas inflow (or outflow) in high-density environment, or gas stripping effect induced by some environmental mechanisms in clusters or groups. Therefore, the possible environmental dependence in the MZR for green-valley galaxies reported here suggests that there might be some environmental mechanisms acting on gas component of galaxies in their quenching phase, which is consistent with our favored mechanism discussed

in this thesis (see Section 4.2).

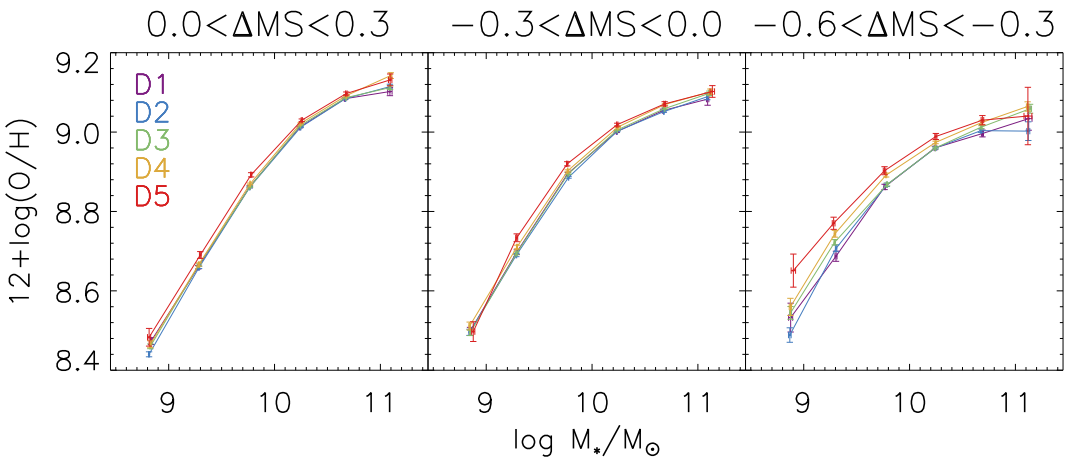

Figure A.1: Mass–metallicity relation for the three ΔMS subsamples. For each panel, we further split the sample into five environmental bins (D1–D5) as indicated in the left panel.

Bibliography

Abadi, M. G., Moore, B., & Bower, R. G. 1999, MNRAS, 308, 947

Abazajian, K. N., Adelman-McCarthy, J. K., Agüeros, M. A., et al. 2009, ApJS, 182, 543

Accurso, G., Saintonge, A., Catinella, L., et al. 2017, MNRAS, 470, 4750

Baldwin, J. A., Phillips, M. M., & Terlevich, R. 1981, PASP, 93, 5

Bolatto, A. D., Wolfire, M., & Leory, A. K. 2013, ARA&A, 51, 207

Boselli, A., Gavazzi, G., Lequeux, J., et al. 1997, A&A, 327, 522

Boselli, A., & Gavazzi, G. 2006, PASP, 118, 517

Boselli, A., Cortese, L., Boquien, M., et al. 2014, A&A, 564, A67

Brinchmann, J., Charlot, S., White, S. D. M., et al. 2004, MNRAS, 351, 1151

Brown, T., Catinella, B., Cortese, L., et al. 2017, MNRAS, 466, 1275

Bruzual, G., & Charlot, S. 2003, MNRAS, 344, 1000

Casoli, F., Boissie, P., Combes, F., et al. 1991, A&A, 249, 359

Catinella, B., Schiminovich, D., Cortese, L., et al. 2013, MNRAS, 403, 683

Chung, A., van Gorkom, J. H., Kenny, J. D. P., et al. 2009, AJ, 138, 1741

Corbelli, E., Bianchi, S., Cortese, L., et al. 2012, A&A, 542, 32

Cortese, L., Catinella, B., Boissier, S., et al. 2011, MNRAS, 415, 1797

Daddi, E., Dickinson, M., Morrison, G., et al. 2007, ApJ, 670, 156

Downes, D., & Solomon, P. M. 1998, ApJ, 507, 615

Dressler, A. 1980, ApJ, 236, 351

Ebeling, H., Stephenson, L. N., & Edge, A. C. 2014, ApJ, 781, 40

Egusa, F., Kohno, K., Sofue, Y., et al. 2009, ApJ, 697, 1870

Elbaz, D., Daddi, E., Le Borgne, D., et al. 2007, A&A, 468, 33

Elmegreen, D. M., Elmegreen, B. G., Frogel, J. A., et al. 2002, AJ, 124, 777

Faber, S. M., Willmer, C. N. A., Wolf, C., et al. 2007, ApJ, 665, 265

Fumagalli, M., & Gavazzi, G. 2013, A&A, 490, 571

Fumagalli, M., Krumholz, M. R., Prochaska, J. X., et al. 2009, ApJ, 697, 1811

Gallazzi, A., Charlot, S., Brinchmann, J., et al. 2005, MNRAS, 362, 41

Genzel, R., Tacconi, L. J., Lutz, D., et al. 2015, ApJ, 800, 20

Giovanelli, R. G., & Hynes, M. P. 1985, AJ, 90, 2445

Gómez, P. L., Nichol, R. C., Miller, C. J., et al. 2003, ApJ, 584, 210

Goto, T., Yamauchi, C., Fujita, Y., et al. 2003, MNRAS, 346, 601

Gunn, J. E., & Gott, J. R., III 1972, ApJ, 176, 1

Hopkins, P. F., & Hernquist, L. 2010, MNRAS, 402, 985

Jablonka, P., Combes, F., Rines, K., et al. 2013, ApJ, 557, A103

Jaskot, A. E., Oey, M. S., Salzer, J. J., et al. 2015, ApJ, 808, 66

Jason, T., Molly, S. P., & Jessica, K. W. 2016, ARA&A, 55, 389

Kamazaki, T., Okumura, S. K., Chikada, Y., et al. 2012, PASJ, 64, 29

Kauffmann, G., Heckman, T. M., White, S. D. M., et al. 2003, MNRAS, 341, 33

Kawada, M., Baba, H., Barthel, P. D., et al. 2007, PASJ, 59, 389

Kenney, J. D. P., & Young, J. S. 1989, ApJ, 344, 171

Kennicutt, R. C. 1998, ApJ, 498, 541

Kewley, L. J., Heisler, C. A., Dopita, M. A., et al. 2001, ApJS, 132, 37

Kewley, L. J., & Ellison, S. L. 2008, ApJ, 681, 1183

Kilborn, V. A., Forbes, D. A., Barnes, D. G., et al. 2009, MNRAS, 400, 1962

Koyama, Y., Smail, L., Kurk, J., et al. 2013, MNRAS, 434, 423

Koyama, Y., Kodama, T., Hayashi, M., et al. 2015, MNRAS, 453, 879

Kroupa, P. 2001, MNRAS, 322, 231

Larson, R. B., Tinsley, B. M., & Caldwell, C. N. 1980, ApJ, 237, 692

Lavezzi, T., & Dickey, J. 1998, AJ, 115, 405

Lee, J. C., Hwang, H. S., Ko, J., et al. 2013, ApJ, 774, 62

Lee, B., Chung, A., Tonnesen, S., et al. 2017, MNRAS, 466, 1382

Lewis, I., Balogh, M., De Propris, R., et al. 2002, MNRAS, 334, 673

Matsuki, Y., Koyama, Y., Nakagawa, T., et al. 2017, MNRAS, 466, 2517

Maier. C., Kuchner, U., Ziegler, B. L., et al. 2016, A&A, 509, 108

Mok, A., Wilson, C. D., Golding, J., et al. 2016, MNRAS, 456, 4384

Mok, A., Wilson, C. D., Knapen, J. H., et al. 2017, MNRAS, 467, 4282

Moore, B., Katz, N., Lake, G., et al. 1996, Nature, 379, 613

Nakajima, T., Kimura, K., Nishimura, A., et al. 2013, PASP, 125, 252

Nakanishi, H., Kuno, N., Sofue, Y., et al. 2006, ApJ, 651, 804

Noeske, K. G., Weiner, B. J., Faber, S. M., et al. 2007, ApJL, 660, L43

Peng, Y.-j., Lilly, S. J., Kovač, K., et al. 2010, ApJ, 721, 193

Peng, Y., Maiolino, R., & Cochrane, R. 2015, Nature, 521, 192

Pettini, M., & Pagel, B. E. J. 2004, MNRAS, 348, 59

Rasmussen, J., Bai, X., Mulchaey, J. S., et al. 2012, ApJ, 747, 31

Saintonge, A., Kauffmann, G., Kramer, C., et al. 2011, MNRAS, 415, 32

Saintonge, A., Tacconi, L. J., Fabello, S., et al. 2012, ApJ, 758, 73

Saintonge, A., Catinella, B., Cortese, L., et al. 2016, MNRAS, 462, 1749

Saintonge, A., Catinella, B., Tacconi, L. J., et al. 2017, ApJS, 233, 22

Scott, T., Usero, A., Brinks, E., et al. 2013, MNRAS, 429, 221

Serra, P., Oosterloo, T., Morganti, R., et al. 2012, MNRAS, 422, 1835

Shimakawa, R., Kodama, K., Tadaki, K., et al. 2014, MNRAS, 441, 1

Solomon, P. M., Downes, D., Radford, S. J. E., et al. 1997, ApJ, 478, 144

Speagle, J. S., Steinhardt, C. L., Capak, P. L., et al. 2014, ApJS, 214, 15

Spitzer, L. J., & Baade, W. 1951, ApJ, 113, 413

Takeuchi, T. T., Buat, V., Heinis, S., et al. 2010, A&A, 514, A4

Tremonti, C. A., Heckman, T. M., Kauffmann, G., et al. 2004, ApJ, 613, 898

van den Bergh, S. 1991, PASP, 103, 390

van de Voort, F., Bahé, Y. M., Bower, R. G., et al. 2017, MNRAS, 466, 3460

Valluri, M., & Jog, C. J. 1990, ApJ, 357, 367

Yang, X., Mo, H. J., van den Bosch, F. V., et al. 2007, ApJ, 671, 153

York, D. G., Adelman, J., Anderson, J. E., Jr., et al. 2000, ApJ, 120, 1579

Acknowledgment

Firstly, I would like to express my deep gratitude to my supervisor Hideo Matsuhara for giving me the opportunity to study the galaxy evolution, as well as his continuous support and encouragement. Besides, I would also like to express my deep gratitude to Yusei Koyama for his enormous and insightful comments, and further he was kindly checked my English many times. It is no exaggeration to say that I have completed this thesis thanks to his support.

I would like to express my gratitude to the members of GENCI project: Takuji Yamashita, Kana Morokuma, Takao Nakagawa, Masao Hayashi, Tadayuki Kodama, Rhythm Shimakawa, Tomoko Suzuki, Ken-ichi Tadaki, Ichi Tanaka and Moegi Yamamoto for their cooperation for NRO45m observation and useful comments for my paper. I also would like to express my thanks to other LIRA members at ISAS, especially Hitomi Kimura for her support of my study life.

I would like to thank the referees of this thesis, Tadayasu Dotani, Nobuyuki Kawai, Hideko Nomura, Kentaro Somiya and Shinya Komugi for their relevant comments, which have improved this thesis.

Finally, I would like to express my deepest gratitude to my parents for their continuing support and worm encouragement.